EFFECTS OF GREAT PLAINS IRRIGATION

ON REGIONAL CLIMATE

BY

David Huber

Submitted to the graduate degree program in Geography and the Graduate Faculty

of the University of Kansas in partial fulfillment of the requirements for the degree of

Master of Science.

_____

David Mechem
Chairperson

_____

Nathaniel A. Brunsell
Co-Chairperson

_____

Johannes J. Feddema

Date Defended: 19 July 2011

The Thesis Committee for David Huber
certifies that this is the approved version of the following thesis:

EFFECTS OF GREAT PLAINS IRRIGATION

ON REGIONAL CLIMATE

_____
David B. Mechem
Chairperson

_____
Nathaniel A. Brunsell
Co-Chairperson

_____

Date approved: 19 July 2011

ABSTRACT

Irrigation provides a much needed source of water in regions of low precipitation such as the western Great Plains. However, adding water to a region that would otherwise see little natural precipitation has ramifications for the partitioning of radiative and turbulent fluxes, the development of the planetary boundary layer, and the transport of water vapor from the regions of irrigation. The first two effects have the potential to drastically alter the climate of irrigated regions of the Great Plains, while the transport mechanism can alter precipitation processes of regions far downstream of the irrigated areas. These effects are investigated in this thesis through the employment of the Advanced Research (ARW) implementation of the Weather Research and Forecasting Model (WRF) version 3.1.1 using a pair of simulations representing an irrigated and non-irrigated Great Plains. It will be shown that the introduction of irrigation in the Great Plains alters the radiation budget by increasing latent heat flux and cooling the surface temperatures. These effects, in turn, provide additional moisture to the atmosphere and increases the net radiation at the surface, thus increasing moist static energy in the boundary layer and providing downstream convective systems with additional energy and moisture. The increase in atmospheric moisture nearly doubles precipitation accumulations downstream without producing any new precipitation events.

ACKNOWLEDGEMENTS

CONTENTS

Chapter 1

Introduction

Many regional anthropogenic impacts on climate are still not well understood and so are often neglected in climate and weather scenarios. The impacts of land cover change make it a first-order climate forcing at local and regional scales (Hansen et al.,2005; Pielke, 2005). Some land cover changes have well understood implications, such as the urban heat island (Arnfield, 2003), whereas others like the effect of clouds on climate (Stephens, 2005) remain elusive. Irrigating croplands in regions where the precipitation is well below the water requirements of the crops has the potential to drastically alter the water and energy balances of those areas (Pielke, 2001). A large portion of the climate community is devoted to the investigation of global influences, specifically greenhouse gasses as modeled in the International Panel on Climate Change's Action Report 4 (IPCC AR4; Solomon et al., 2009; Cook et al., 2008). However, the irrigation of cropland in semiarid regions can have impacts on local and regional scales comparable to the influence of increased greenhouse gasses (Brunsell et al., 2010). The task of modeling the temporal variability of soil moisture under irrigated regimes is one of considerable difficulty, because the variability associated with farmers applying irrigation at different

times of the growing season is a function of precipitation patterns and personal
preference of individual farmers.

Irrigation has long been looked at as a source for enhanced precipitation downstream
(Barnston and Schickedanz 1984), but attempts to study the impacts have relied heavily
on statistical methods (e.g. Moore and Rojstaczer 2002; Barnston and Schickedanz 1984),
short-term case analyses (e.g. DeRidder and Gallée 1998; Lohar and Pal 1995), or longer
scale GCM analyses (e.g. Boucher et al. 2004; Kueppers et al. 2007; Sacks et al., 2009).
Although a statistical approach provides evidence of an association between irrigation
and significant changes to storm tracks and intensities, the mechanisms that irrigation
might affect convective precipitation processes cannot be understood using only
statistical methods.

One problem with performing short-term case studies on irrigation is that water vapor
provided by irrigation varies greatly depending on the crop type, the temporal variability
of naturally occurring precipitation, and time of the growing season, which cannot be
fully resolved in a short-term study. Thus, the long-term, large-scale statistical studies
are often more revealing than the short-term numerical simulations. This problem has
started to be addressed by recent studies which perform longer-term simulations
(including Adegoke et al. (2003), who performed a 15 day integration over Nebraska).
However, a longer-term (>10 days), fine-scale RCM study that covers a large
geographical area ($>10^6$ km^2) has yet to be performed on the impacts of irrigation on
precipitation. The incorporation of all scales from meso-γ (2-20 km) to synoptic is
important in the case of irrigation due to the nature of nearly point-source irrigation

influencing micro- and mesoscale circulations, whereas large-scale irrigation has the potential to influence continental precipitation patterns and radiation budgets.

This thesis investigates the mechanisms that alter the radiation budget and support enhanced precipitation as related to irrigation. To address the longer term variability associated with irrigation, a three month long pair of integrations of a three-dimensional, non-hydrostatic model are performed. In order to investigate the effects on various scales, the study region encompasses the majority of the United States and is performed on a 12 km mesh — fine enough to resolve the mesoscale, and a large enough domain to resolve synoptic scale processes. Specific mechanisms of interest to the study are those related to the radiation balance, the Great Plains Low Level Jet (GPLLJ), and convective potential.

Chapter 2

Theory of Irrigation's Influence on Climate

This chapter will discuss, on a theoretical level, the impacts of irrigation. Specific

interest of this chapter will be focused on the influences of irrigation on the climate of the

Great Plains. In order to do this effectively, a discussion in section 2.1 on the Great

Plains climate and summertime convective systems will be presented. Following this,

section 2.2 will discuss the impacts of irrigation on the surface energy balance, section

2.3 will summarize the effects on the boundary layer, and section 2.4 will illustrate how

irrigation may influence precipitation.

2.1 Climatology of the Great Plains

The Great Plains consists of three different climate regimes (Figure 2.1a; Peel et al.,

2007): humid continental in the eastern two-thirds of the northern and central plains (Dfa

and Dfb), humid subtropical in the eastern two-thirds of the southern plains (Cfa), and

semi-arid in the western third of the Great Plains (BSk). The majority of the Great Plains

lies in an east-west precipitation gradient, with the driest climates abutted against the

Rocky Mountains (Figure 2.1 b). Many precipitation events in the Great Plains are

associated with surface cyclones passing through North America and enhanced in the lee

of the Rocky Mountains (Smith, 1984). This process typically takes place from Fall to

Spring when synoptic surface cyclones propagate through the region.
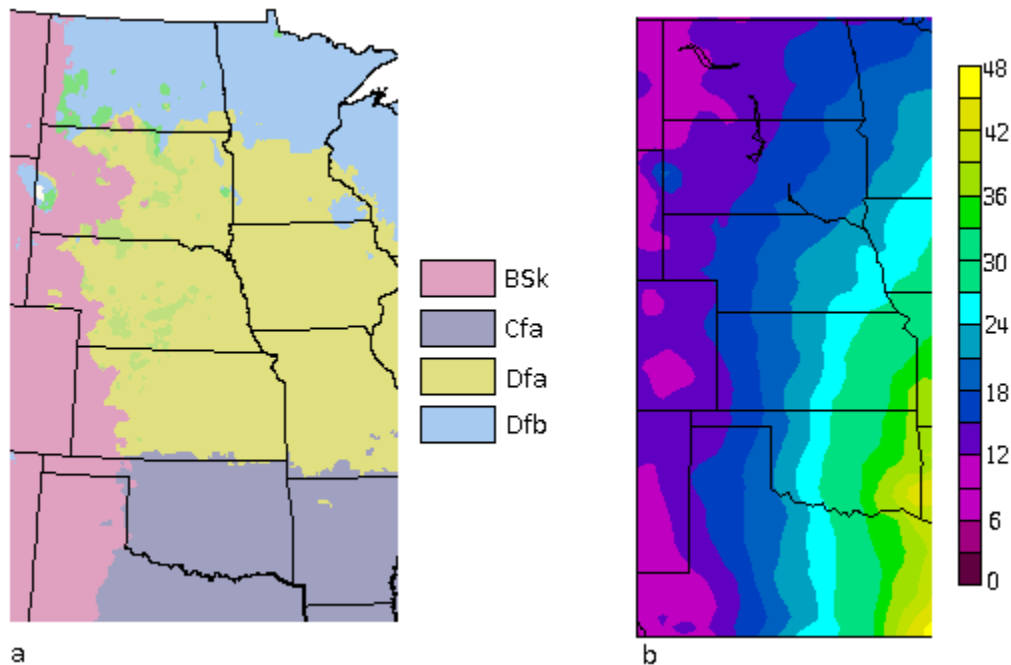
Figure 2.1 a) Climate regions of the Great Plains and western Midwest and b) average (1979-2010) annual accumulations of precipitation (in.) across the Great Plains.

During the Summer, precipitation events take the form of smaller mesoscale

convective systems (MCSs; Fritsch et al., 1986). These events tend to be in regions of

weaker synoptic-scale forcing, with moisture being provided by local evaporation and the

Great Plains Low Level Jet (GPLLJ; Trier et al., 2010). The GPLLJ transports warm,

moist air from the Gulf of Mexico at low levels of the atmosphere — from the surface to

approximately 700 mb — though the GPLLJ is most evident at 850 mb. The speed of the

GPLLJ varies diurnally, with the strongest winds occurring in the overnight hours (0000

to 0600 LST; Arritt et al., 1997) when the surface decouples from the 850-mb level of the

atmosphere, reducing frictional effects on the flow.

Summertime MCSs tend to coincide with the strengthening of the GPLLJ, generally

initiating in the late evening and intensifying overnight, then diminishing in the mid- to

late morning hours (Trier et al., 2010). These MCSs are typically associated with quasi-stationary surface fronts in the vicinity of the exit region of the GPLLJ where low level convergence reaches a maximum (Tuttle and Davis, 2006) and differential temperature advection enhances lower-level lapse rates (Trier et al., 2006).

2.1.1 Irrigation and Agricultural Practices in the Great Plains

The agricultural practices in the Great Plains make it one of the more studied regions for the effects of irrigation on local and regional climate (e.g. Barnston and Schickedanz, 1984; Moore and Rojstaczer, 2001; Kustu, 2011). The low precipitation totals in the western Great Plains require large amounts of irrigation in order for plants to survive in the semi-arid climate (Miller and Appel, 1997). Figure 2.2a shows the average daily well draws of water for irrigation purposes from the Central Plains and Midwest, most of which comes from the Ogallala Aquifer (Figure 2.2b). The practice of irrigation, which is widely used in this region, influences the water budget and radiation balance by introducing more water to the soil, and ultimately the atmosphere, through increased evaporation (Maxwell et al., 2003). In the absence of advective sources like the GPLLJ, the other significant source of atmospheric moisture throughout the Great Plains is evapotranspiration (Higgins et al., 1997; Trier et al., 2010), which is enhanced by irrigation practices (e.g. Adegoke et al., 2003).

2.1.2 Effects of Soil Moisture on Precipitation

Irrigation directly affects soil moisture, which may then exert an influence on precipitation. Several studies (e.g. Jones and Brunsell, 2008; and Findell and Eltahir 2003a,b) have shown that soil moisture and precipitation are linked through either the

enhanced evaporation and moister boundary layers from wet soils or the stronger

boundary layer convection generated by dry soils.

Jones and Brunsell (2008) found that for the Konza Prairie, (located near Manhattan,

KS), a strong positive link between high soil moisture and precipitation was noticeable at

several different horizontal grid spacings (1, 2, 4, 8, and 16 km). This effect was

demonstrated by setting initial soil moisture in each different model resolution to field

capacity (FC), 50% FC, and wilting point (WP). The FC experiments consistently

produced more precipitation, with higher precipitation rates per event, but fewer events

overall than in the 50% and WP cases. Also an important finding in the study by Jones

and Brunsell was that the time it took for this effect to become noticeable was

approximately 14 days.

Findell and Eltahir (2003a,b) developed a framework to identify under what

atmospheric conditions the soil moisture properties would favor convection, and which

regions of the United States fell into each category (favoring either moist soils or dry

soils for convection). They found that areas of relatively high boundary layer moisture

and slightly unstable middle-atmospheric profiles (associated with a relatively weak

capping inversion) tended to favor wet soils for convection. Regions of relatively low

boundary-layer moisture and moderately unstable upper-atmospheric profiles, on the

other hand, favored dry soils. Applying this framework to the Great Plains showed that

summer convection in the region favored either wet or dry soils for convection, since the

Great Plains has highly variable atmospheric conditions. Thus the likelihood of

convection is determined by both soil moisture and lower- to middle-atmospheric

properties. This finding is in agreement with Jones and Brunsell (2008), since both

studies showed that convection can occur with either dry or moist soils. The difference

being that Jones and Brunsell investigated the precipitation totals rather than whether an

event will happen or not, as in the study by Findell and Eltahir.
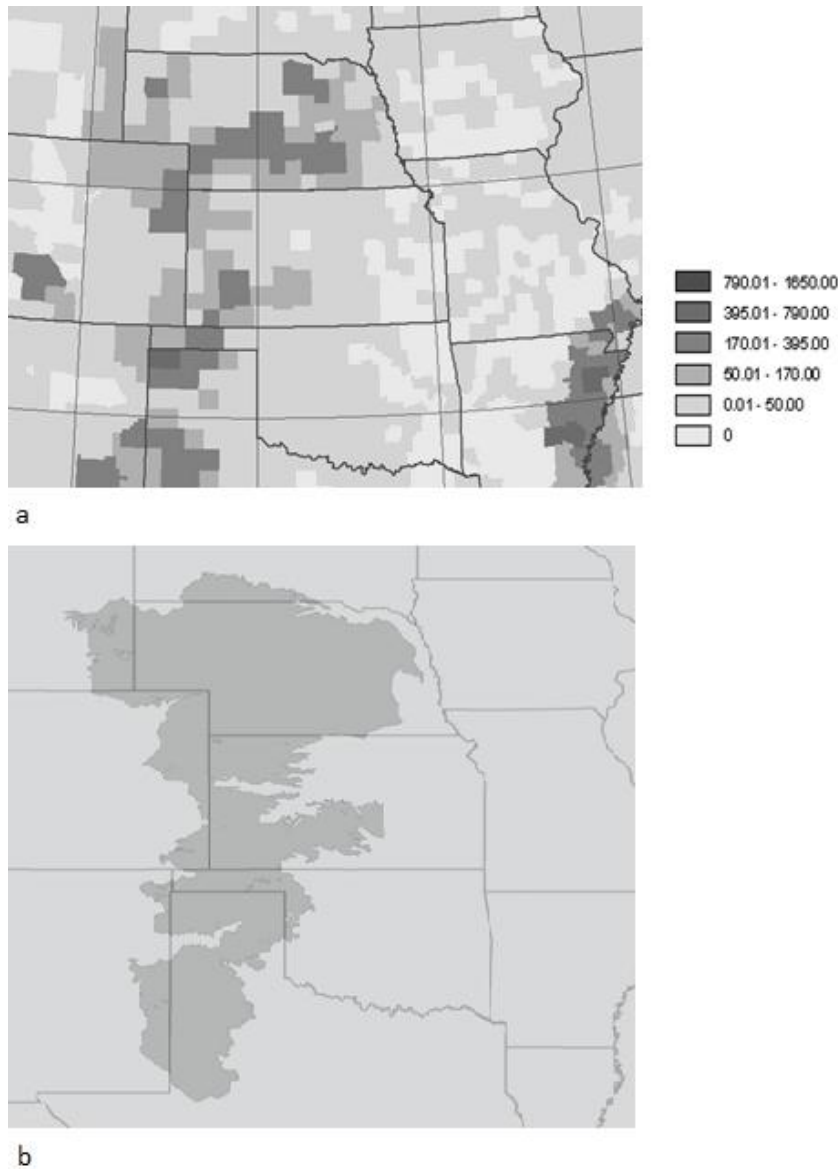
Figure 2.2 a) Irrigation draws for the year 2000 averaged over the growing season (Miller and Appel, 1997). Units are 10^6 Gal d^{-1}. b) Extent of the Ogallala Aquifer (Gutentag et al., 1984).

How soil moisture can influence precipitation is largely determined by atmospheric

properties associated with local, regional, and synoptic scale water vapor, temperature,

and energy and the transport of these quantities. As such, this study aims to quantify how

irrigation throughout the Great Plains and the Midwest modifies these properties. The ability of irrigation to affect moisture transport at many spatial scales makes it a significant source for higher values of atmospheric water content and precipitation, not only locally, but downstream of irrigated regions as well (Boucher et al., 2004).

2.2 Irrigation's Effects on the Surface

Figure 2.3 illustrates a generalized flow chart summarizing the effects of increased soil moisture, such as that provided by irrigation, on the surface radiation budget and precipitation. The surface effects that will be considered here are the alterations to the radiation budget and moist static energy (MSE). The radiation budget is defined by

$$R_n = H + LE + G \tag{2.1}$$

where R_n represents the net radiative fluxes $= \varepsilon LW_d - \sigma \varepsilon T_s^4 + (1 - \alpha)SW$; G is the soil heat flux; H is turbulent sensible heat flux (W m^{-2}); LE is the turbulent latent heat flux (W m^{-2}); SW is the shortwave radiation incident at the surface (W m^{-2}); α is albedo; LW_d is downwelling longwave radiation (W m^{-2}); $(1 - \varepsilon)LW_d - \sigma \varepsilon T_s^4 = LW_u$ is the upwelling longwave radiation (W m^{-2}); σ is the Stephan-Boltzmann constant (W m^{-2} K^{-4}); ε is the emissivity of the surface; and T_s is the surface skin temperature in K. MSE is defined as

$$MSE = c_p T + gz + L_v q \tag{2.2}$$

where c_p is the specific heat of air at constant pressure (J kg^{-1} K^{-1}); T is temperature in K at the height of interest; g is the acceleration due to gravity; z is height (m); L_v is the latent heat of vaporization (J kg^{-1}); and q is the water vapor mixing ratio (kg kg^{-1}).

Adegoke et al. (2003) investigated the impact of irrigation on boundary layer dynamics on a regional scale by employing the Regional Atmospheric Modeling System (RAMS) over a 15 day period in which irrigation was parameterized by setting soil

moisture to field capacity once a day. They also examined climate records from weather stations in irrigated and non-irrigated locations of Nebraska. Results from the model showed a 36% increase in latent heat and a 15% decrease in sensible heat flux between irrigated and non-irrigated runs in Nebraska.

The addition of water through irrigation increases evapotranspiration (*LE*) from the surface soils and plants, decreasing near surface temperatures by the transfer of energy into the evaporation of water instead of increasing molecular energy, thus decreasing H simultaneously (Douglas et al., 2009). The decrease in surface temperatures also decreases *H* since less heat energy is available (Pielke, 2001), while also decreasing upwelling longwave radiation (Eltahir, 1998). The decrease in upwelling longwave radiation associated with the cooler surfaces allows for additional radiation to be partitioned into the two turbulent fluxes, increasing *LE* further since it is favored over *H* (Betts et al., 1994). Moreover, the decreased upwelling longwave radiation from the surface, in combination with the increased greenhouse effect from the additional water vapor in the atmosphere, decreases the range in temperatures since the surface will not cool as quickly at night (Eltahir, 1998).

By increasing evapotranspiration rates, the near surface water vapor mixing ratio also increases (Entekhabi et al., 1996). The additional atmospheric water vapor has the potential to increase MSE, though the decrease in surface temperature has a counteractive effect (Pielke, 2001). In order for MSE to remain unchanged, the change in temperature and the change in mixing ratio must satisfy

$$\delta T = \frac{L}{c_p} \delta q. \tag{2.3}$$

Equation 2.3 implies that for typical Great Plains summertime temperatures and dew

point temperatures, a 1 K increase in surface dew point would require about a 2 K

decrease in surface temperature in order for MSE not to change. In a 15 day long

modeling study comparing irrigated and non-irrigated practices over Nebraska by

Adegoke et al. (2003), it was found that the decrease in temperature (1.2°C) was less than

the increase in dew point temperature (2.6°C). This result suggests that moist soils

provide more energy to the atmosphere than dryer soils, which has the net effect of

increasing near-surface MSE.
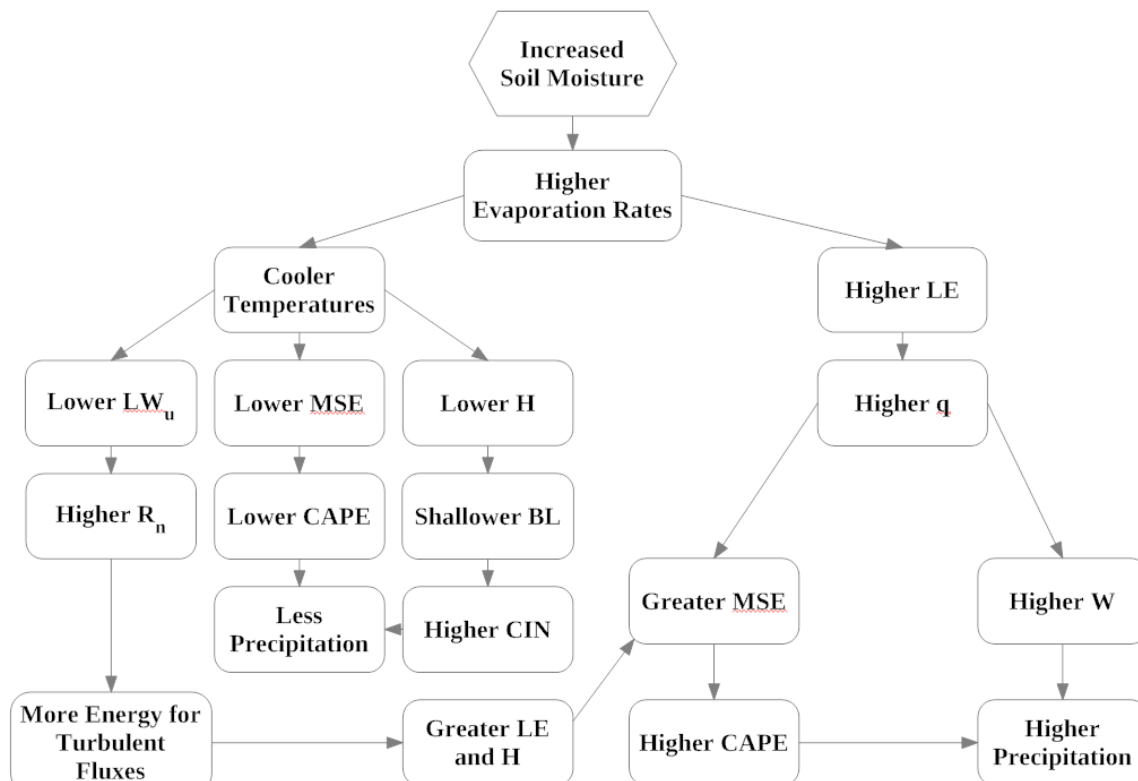
Figure 2.3 Idealized flow chart identifying pathways for irrigation to influence temperature, the boundary layer, and precipitation.

Another possible effect investigated by Twine et al. (2004) is caused by the transition

of land cover from natural vegetation to irrigated agriculture. Depending on the type of

natural foliage in place before agriculture, α may be altered, which would affect the

shortwave radiation at the surface. For instance, moving from a forested canopy to cropland was shown to decrease net radiation due to the higher albedo of the cropland, especially during the winter when snow cover and/or barren land were prominent in the cropland. Other scenarios, such as moving from grassland to crop land saw little effect in the net radiation since albedo did not change much, indicating that the type of land cover change is important in determining how it will affect regional climate.

2.3   Irrigation and the Boundary Layer

In the presence of irrigation, the surface fluxes are altered, with preference given to *LE* over *H*. The decrease in *H* results in a much shallower boundary layer, as implied by the equation (Deardorff, 1974)

$$\frac{\partial z_i}{\partial t} \sim H^{2/3} z_i^{-4/3} \tag{2.4}$$

where z_i is the height of the boundary layer. The decrease in *H* also decreases the amount of air entrained into the boundary layer from the free troposphere, which implies that the capping inversion is more slowly eroded (Deardorff, 1974). However, the increase in boundary layer water vapor and MSE results in parcels reaching the lifting condensation level (LCL) and the level of free convection (LFC), respectively, lower in the atmosphere (Pielke, 2001). This means that the parcel's equivalent potential temperature (θ_e) might be warm enough that it passes through the capping inversion in a positively buoyant state (Findell and Eltahir, 2003a). Additionally, the decreased *H* from the surface results in less entrainment of the dry, free-atmospheric air into the boundary layer. The higher θ_e of the parcel, associated with greater MSE, is also generally associated with greater CAPE (Pielke, 2001). Because there is less dry air entrainment, the boundary layer experiences less dilution of MSE, keeping the boundary layer air more unstable than if *H*

were higher. Betts et al. (1994) showed this effect to be a key feature in the extensive flooding over the Midwestern U.S. in 1993, where high soil moisture from record rainfall reduced H and maintained boundary layer MSE through less dilution from free-tropospheric air.

The presence of horizontal soil moisture heterogeneity, such as locations of irrigated land cover next to non-irrigated land cover, results in spatially-variable boundary layer depths and vertical profiles of temperature and moisture. This heterogeneity generates solenoidal, mesoscale circulations resembling land-sea breezes, transporting the moist air from the irrigated regions to the dryer regions where it rises (Avissar and Liu, 1996). The result is upward motion over the dry, warm surface and downward motion over the moist, cool surface caused by outflow of air from the regions of moist soils (Clark and Arritt, 1995). This leads to the advection of moist, higher-MSE air to the drier regions where values of H are greater and the capping inversion of the boundary layer is more quickly eroded (Deardorff, 1974). The transport of the higher-MSE air over the irrigated regions to the non-irrigated regions should increase CAPE while decreasing CIN, because the higher MSE air has a higher θ_e (Pielke, 2001).

This effect was investigated by Avissar and Liu (1996) in an idealized simulation of "checkerboard" soil moisture patterns, with several regions of high soil moisture surrounding grid cells of low soil moisture. The simulations showed that inflow from the high soil moisture grid cells into the dry soil moisture grid cells provided significant convergence and lift over the moist grid cells, producing several high precipitation events.

While enhanced evapotranspiration has obvious implications for local water budgets and transport, it may also have implications for the regional atmospheric circulation as well. As shown by Paegle et al. (1996) in a modeling study of the flood of 1993, enhanced evaporation over the Great Plains during the summer months weakened the GPLLJ. This suggests that irrigation may have long-term effects on precipitation processes across the Great Plains, and not just near irrigated locations.

2.4   Irrigation's Influence on Precipitation

When considering the Great Plains, the location of the irrigation is important when determining how it will affect precipitation. The addition of water vapor through irrigation to the south of the low level convergence zone discussed in section 2.1 increases the moisture advection to the convergence zone, likely increasing the total precipitation of an MCS propagating through the region. Additionally, the location of the GPLLJ exit region with respect to soil moisture heterogeneity could provide additional low-level convergence and associated upward vertical motion. For instance, consider Figure 2.4a where an idealized situation of the GPLLJ overlaying agricultural and dry lands is shown. In Figure 2.4a, the exit region of the jet coincides with the southern edge of the irrigated agriculture. The tendency of the air at the surface is to travel from the lower values of H overlying the agriculture to the more convectively active boundary layers to the south. This result is more likely to initiate or maintain an MCS than if the values of H were the same in both regions, as shown in Figure 2.4b.

Irrigation can also reduce the amount of precipitation overtop the irrigated regions that are adjacent to regions of dry soils. This would be the result of the mesoscale circulation, which has the net effect of decreasing upward vertical motion or increasing

downward vertical motion. If the jet exit region is aligned overtop the irrigated agriculture, the likelihood of an event would be reduced, but the total amount of precipitation would likely increase because of the higher boundary layer moisture (Jones and Brunsell, 2008).

A number of studies have investigated the effects of irrigation on precipitation. Focusing on irrigation in the Texas panhandle, Barnston and Schickedanz (1984) performed statistical studies on the influence of irrigation on rainfall downstream of irrigated sites. They used principal components analysis (PCA) to determine if irrigation had a significant influence on precipitation when synoptically driven disturbances produced low level convergence and lift. The need for low level convergence was a key part of the study, since the low-level flows deliver the additional moisture from irrigation. Barnston and Schickedanz found that surface warm fronts, stationary fronts, and low pressure centers were the largest contributors to precipitation downstream of irrigated regions, with a statistically significant effect only in specific years when precipitation was abnormally high in June or July.

Moore and Rojstaczer (2002) investigated the impacts of irrigation on precipitation anomalies within a 400×400 km^2 area of the Texas panhandle. They did so by identifying areas of anomalously high precipitation in individual precipitation events via radar imagery for the summers of 1996 and 1997, then calculating the magnitudes of the anomalies with raingauge data. Moore and Rojstaczer found a contribution from irrigation of between 6 and 18% of rainfall downstream, with a maximum effect within the analysis area about 90 km away. They also noted that approximately 10% of the water evaporated by irrigation was returned in the sampling area from precipitation

during these events. This suggests that many of the possible impacts of irrigation could

be located much further downstream of the actual irrigated locations.
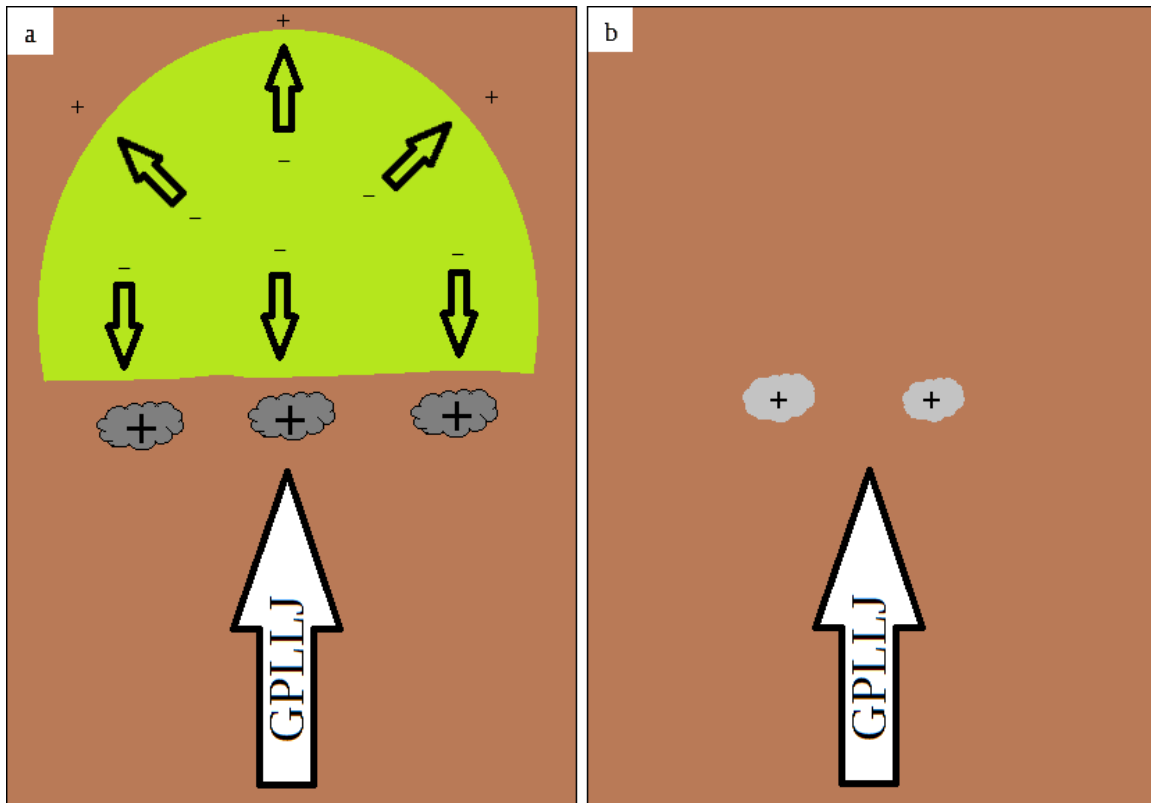
Figure 2.4 Idealized representation of the convergence zone associated with the GPLLJ (a) in the presence of irrigated agriculture and (b) without irrigation. Green areas are representative of irrigated agriculture, while brown areas represent areas of dry land cover. Small arrows over the irrigated agriculture are indicative of the near-surface flows resulting from the solenoidal circulations discussed in section 2.3. The '+' and '–' indicate areas of upward or downward vertical motion, respectively, with the size of each representing the relative magnitude of the vertical motion associated with the jet exit region, the solenoidal circulations, or both.

Other portions of the world have also seen the influence of irrigation on precipitation.

Lohar and Pal (1995) investigated the effects of irrigation on convection in Bengal, India,

where irrigation occurs along much of the eastern coastline adjacent to the Indian Ocean.

They used a simple two-dimensional model, and parameterized irrigation by holding soil

moisture at field capacity throughout the experiment.   Lohar and Pal reported that the

decreased temperature gradient between land and sea caused by enhanced evaporative

cooling from irrigation decreased premonsoon convection due to a weakened land-sea

breeze. At the same time, a circulation very similar to a land-sea breeze, except located between the non-irrigated and irrigated land coverages, was observed in their model results.

In another two-dimensional modeling study, DeRidder and Gallée (1998) focused on irrigated lands in Israel. DeRidder and Gallée used their model to identify effects on precipitation, surface cooling, and moisture flux throughout the troposphere. In their study, it was found that irrigation increased the probability of precipitation during a period when very little rainfall was recorded, and that irrigation led to lower surface temperatures and less intense vertical mixing at the top of the boundary layer from lower values of *H*.

Chapter 3

Methodology

To ascertain the effects of irrigation on the flow, radiation balance, and precipitation over the Great Plains and Midwest, two simulations (hereafter Control and Irrigated) were performed using the Advanced Research (ARW) implementation of the Weather Research and Forecast Model (WRF) version 3.1.1, a three-dimensional, non-hydrostatic, fully compressible numerical model (Skamarock et al., 2005). The simulations used the physical and dynamical options as summarized in Table 3.1. Initial conditions and 3-hourly boundary conditions for both simulations were provided by the 12-km North American Mesoscale Model (NAM, formerly known as the Eta model; Black, 1994). Both simulations were initialized on 1 May 2001 and integrated through 31 July 2001. The spin-up period for each simulation ended 0000 UTC, 1 June 2001. Both model runs were simulated on a 12-km mesh spanning most of the United States (Figure 3.1a) and employed a 30-s time step. This time period was chosen because the global signals (e.g. the El Niño Southern Oscillation, ENSO) for the period are nearly neutral, the soil moisture content of the Great Plains soils were close to the climatic average, and the

strength and position of the GPLLJ were typical for the summer period (Trier et al., 2010). Trier et al. (2010) discuss the overall synoptic features and forcing mechanisms supporting convection through the period, though they do not address the presence of irrigation.

Table 3.1 Some of the key parameterizations and grid information for the domain used for both simulations.

Grid Spacing	12 km $\times$ 12 km
Grid Points	300 east-west $\times$ 224 north-south $\times$ 48 vertical
Time Step	30 s
Land Surface Model	Noah LSM Version 3.1 with 4 soil levels
Planetary Boundary Layer Scheme	Yonsei University PBL
Convective Parameterization	Kain-Fritsch
Boundary Conditions	3-Hourly NAM
Initial Conditions	NAM
6th Order Diffusion Coefficient	0.12
Vertical Spacing	17 levels below 1 km, increasingly spaced above the boundary layer and 6 levels in the top 50 mb

Both simulations used a modified 24-category USGS land cover scheme to identify regions of irrigation. The land cover was modified with the specific intent of better identifying regions of irrigated agriculture overlying the Ogallala Aquifer in the Great Plains. The majority of the irrigated land cover added to the USGS land cover scheme is circled in Figure 3.1. The land cover scheme was altered to better quantify the maximum effect of irrigation in two ways: 1) grid cells containing any amount of irrigated land as identified by the original USGS land cover classification were set to contain only irrigated land and 2) cells overlying the Ogallala aquifer that contained any amount of the land cover type "grassland/agriculture mosaic" were set to contain only irrigated land. The algorithm used in the original USGS land cover scheme identifies cells containing agriculture (irrigated and/or dry) and grassland as grassland/agriculture mosaic

(Anderson et al., 1976), so the assumption was made here that any land cover of this type overlying the Ogallala aquifer is irrigated agriculture.
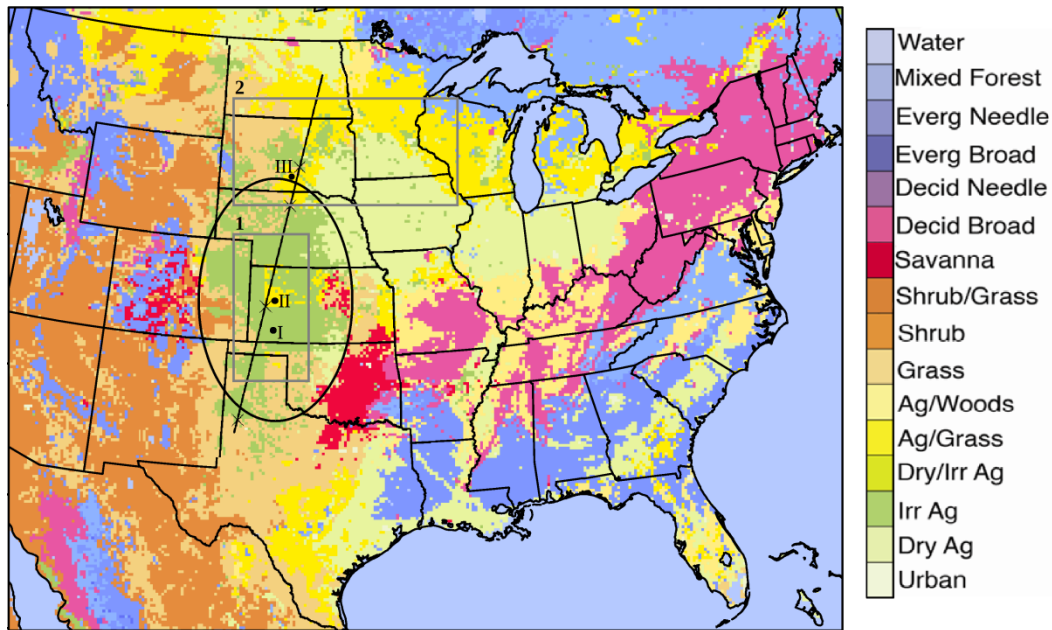

Figure 3.1 Study domain showing land cover classification scheme used for all model cases. The line represents the location of the cross-section analyzed in section 4.4 on which the Xs indicate regions of contrast in land cover types, from an irrigated land cover to a non-irrigated land cover, which are used for reference in Figures 4.10 a-c. Points labeled I, II, and III are analyzed using skew-T diagrams in section 4.3. Regions labeled 1 and 2 represent the irrigated and downstream regions, respectively, and are examined separately in Section 4.6.

Although the irrigated area identified in Figure 3.1 does not match the exact shape of the Ogallala aquifer (Figure 2.2b), it does capture the majority of the features of the aquifer and the use of water for irrigation purposes (Figure 2.2a). The region of agriculture/grassland mosaic in northwestern Kansas was chosen to remain as such to better simulate the regions of Kansas where dryland agriculture and natural grasslands dominate the landscape. Although this relatively small region does not match the exact shape and location of the actual dry agricultural landscape, its size is approximately the same (Figure 3.2). Moreover, the synoptic scale features and prevailing surface to 850 mb winds in the region are nearly identical. These simulations are not intended to match

observations, but rather to identify potential impacts of irrigation. One such impact is possible to occur in northwestern Kansas due to the spatial heterogeneity of land cover and correlated high contrasts in soil moisture profiles.

The difference between the simulations is the treatment of irrigation. In Control, soil moisture is only replenished by precipitation, or surface and subsurface flow of groundwater. Irrigated was exactly the same, except that the code of WRF was modified to account for irrigation. Starting 15 May at 0000 UTC of the simulation, the soil moisture content of the top meter of soil for irrigated land cover types was set to field capacity. This process was repeated every day thereafter at 0000 UTC until the end of the simulation. The timing of the first simulated irrigation was chosen to occur during the model spin up period to allow enough time for the soil moisture to influence precipitation processes — approximately 14 days (Jones and Brunsell, 2008). Only the top meter of the soil was set to field capacity in the simulation because irrigated land cover types in Noah are assigned rooting depths of 1 m. The two simulations represent the two extremes of agriculture in the Great Plains, presenting the agriculture with no added water or keeping the soils of the Great Plains at maximum evaporative potential.
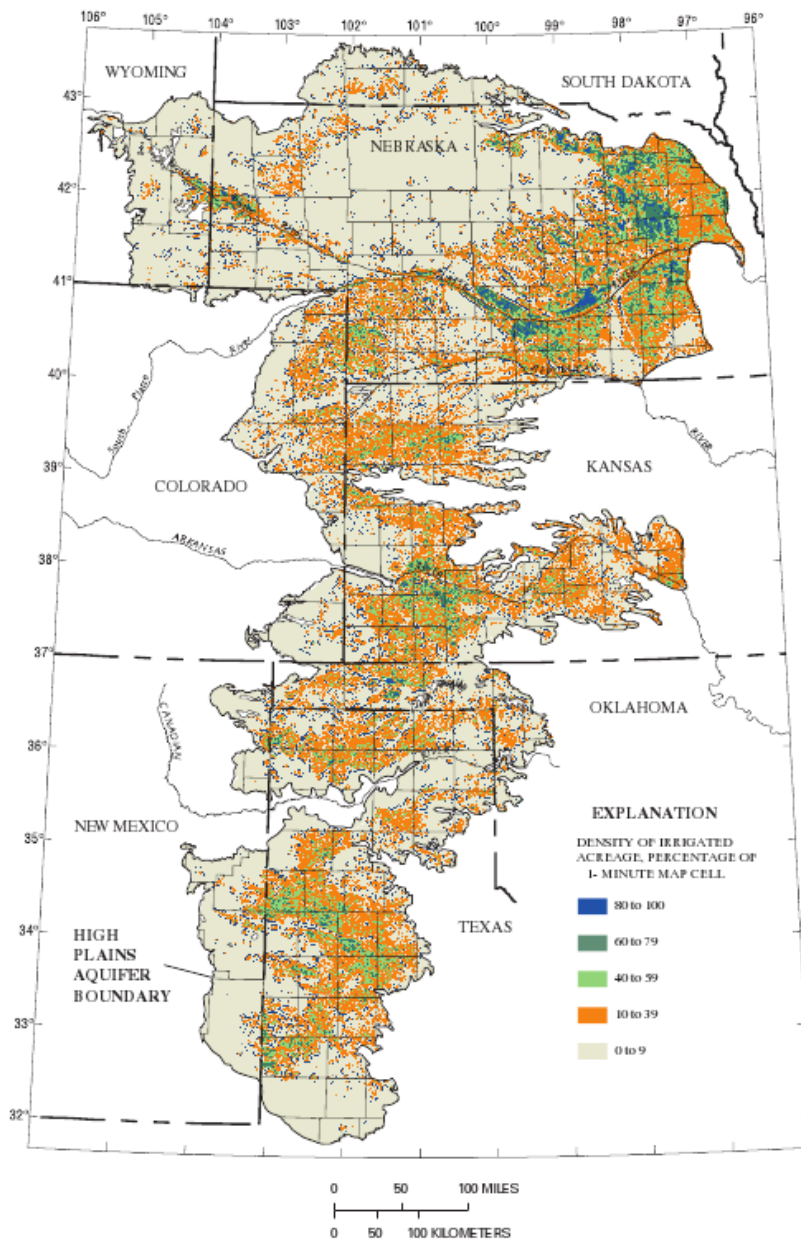
Figure 3.2 Irrigated locations and densities spanning the Ogallala Aquifer for the 2000 growing season, from McGuire et al. (2003). The colors represent the percentage of the land cover occupied by irrigated agriculture with grey representing less than 10%, orange representing 10 to 39%, light green as 40 to 59%, dark green as 60 to 79% and blue representing 80 to 100% of the 1-minute cell being occupied by irrigation.

Chapter 4

Simulation Results

4.1   Introduction

This chapter presents the results of the two simulations discussed in Chapter 3. Most

values, except where otherwise specified, are expressed as monthly mean differences

between Irrigated and Control. The differences in soil moisture between Control and

Irrigated are most dramatic in the month of July. For this reason, results are only

presented for July. As a result of the decreased soil moisture in Control, the driving

mechanism for the changes seen in this experiment is the change in the top meter of soil

moisture over the irrigated land cover types. Section 4.2 discusses the differences in the

radiation budget between Irrigated and Control. Section 4.3 presents the different

thermodynamic structures of the atmosphere for points I, II, and III, identified in Figure

3.1. Sections 4.4 and 4.5 discuss differences between the lower atmospheric flow and

precipitation, respectively, between Irrigated and Control. Finally, section 4.6 discusses

the spatially averaged differences between Irrigated and Control in regions 1 and 2, as

identified in Figure 3.1.

4.2   Effects on the Radiation Budget

The surface radiation budget equation used in this thesis is described by equation 2.1. The factors ε and α are held constant by WRF for each land cover type across both simulations, except in the presence of snowpack or sea ice, which are beyond the scope of this study. Since WRF does not alter ε or α according to differing amounts of soil moisture, it is assumed that differences in the terms of the radiation budget are based on other factors.

As shown in Figure 4.1a and b, the difference in hourly averaged latent heat flux between the Irrigated and Control case for July is dramatically higher over the irrigated regions of the Great Plains (region 1, Figure 3.1a), as well as to the north of the irrigated regions to a lesser extent (region 2, Figure 3.1a). The ~100 to 400% increase in LE over the irrigated regions is a result of increased evapotranspiration from the nearly-saturated irrigated land cover as compared to the more arid soil of Control, while the increased flux to the north of the irrigated region is due to an increase in precipitation, which moistens the soil, increasing evapotranspiration and recycling the water provided from irrigation. In Figure 4.1c and d, a large decrease in sensible heat flux (~25 to 100%) is apparent, though slightly less in magnitude than the increase in latent heat flux. This change in sensible heat flux is driven by decreased temperatures from evaporative cooling (Figure 4.2) and more energy being devoted to evaporation that surface heating. The change in hourly averaged July G (not shown) is slightly positive, though small (< 1 W m^{-2} in most areas), over most of the irrigated regions.

Evaporative fraction (EF) is defined as

$$EF = \frac{LE}{R_n - G}.$$
(4.1)

EF represents the amount of turbulent flux energy partitioned into the evaporation of water into the atmosphere. Figure 4.1e shows the daily averaged differences in evaporative fraction between Irrigated and Control. As ascertained by this figure, the amount of energy at the surface used to evaporate water is markedly higher Irrigated than Control over the irrigated regions. This is especially true in the southern portions of the irrigated agriculture where nearly 60% more energy is devoted to the evaporation of water in Irrigated than in Control.

The differences in daily averaged maximum and minimum 2-m temperatures are shown in Figures 4.2a and b, respectively. Figure 4.2c depicts the change in daily averaged 2-m diurnal temperature range between Irrigated and Control. These figures indicate that the presence of irrigation decreases surface temperatures across most of the domain due to the increased evapotranspiration and transport of the cooler air. The range in temperatures decreases because the emission of longwave radiation from the surface is lower (Figure 4.3a). The decrease in temperature results in decreased upwelling longwave radiation over much of the irrigated region. Downwelling longwave radiation decreased slightly over much of the region (not shown) due to cooler temperatures of the lower atmosphere being balanced by the increased green house effect, indicating that the majority of the change in net longwave radiation (Figure 4.3b) is from the decreased upwelling longwave radiation.
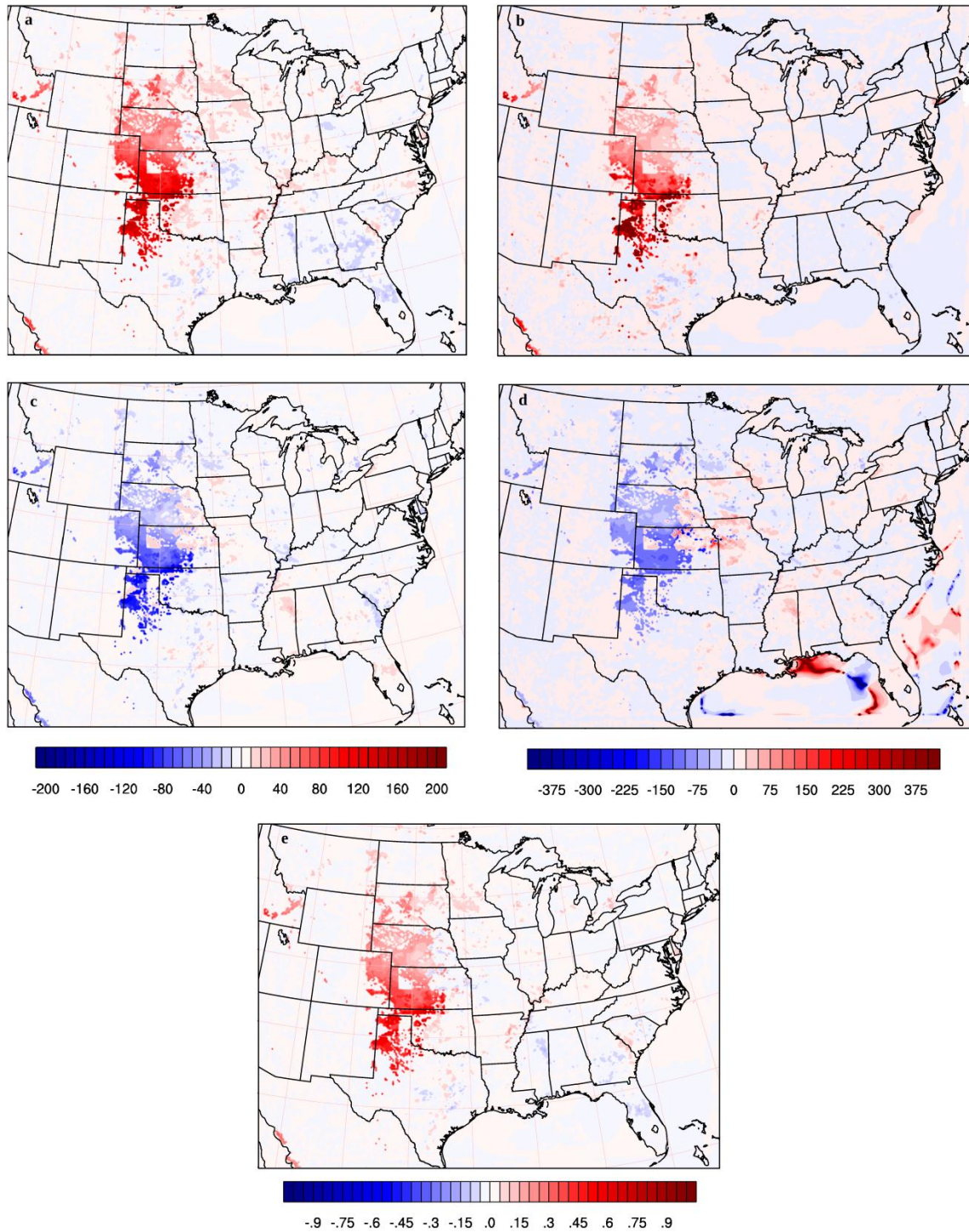
Figure 4.1 Absolute and percent differences in hourly averaged surface (a and b, respectively) latent and (c and d, respectively) sensible heat flux between the Irrigated and Control cases for the month of July with units of W m^{-2}.
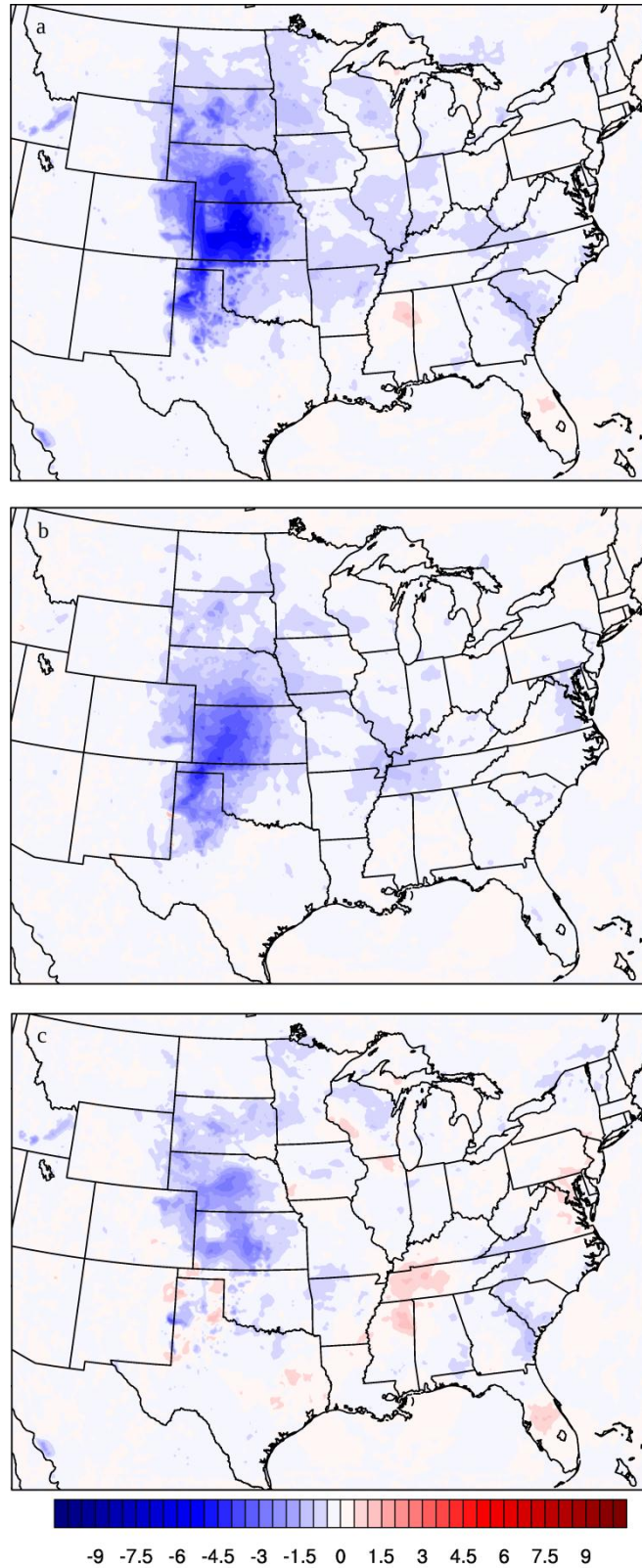
Figure 4.2 July averaged daily mean 2 m temperature (a) maximum, (b) minimum, and (c) range differences between Irrigated and Control. Units for the contours are all in K.

The hourly averaged net shortwave radiation difference is shown in Figure 4.4a. Figure 4.4b depicts the differences between Irrigated and Control net radiation. Since the albedo of the surface does not change, changes in shortwave radiation are only due to changes in cloud cover. This indicates increased cloud cover, and thusly decreased shortwave radiation at the surface, over the northern Great Plains, southwestern Missouri,
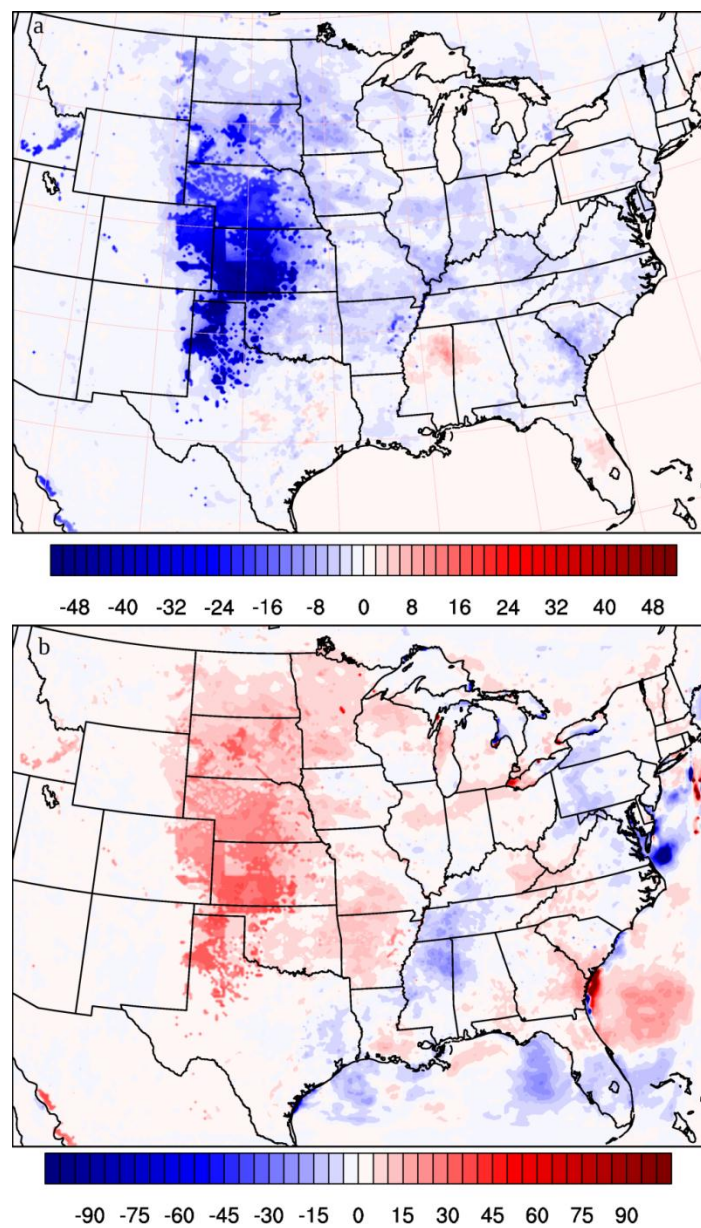
Figure 4.3 (a) July hourly averaged differences in upwelling longwave radiation between Irrigated and Control cases (W m^{-2}). (b) Percent difference in July averaged net longwave radiation.
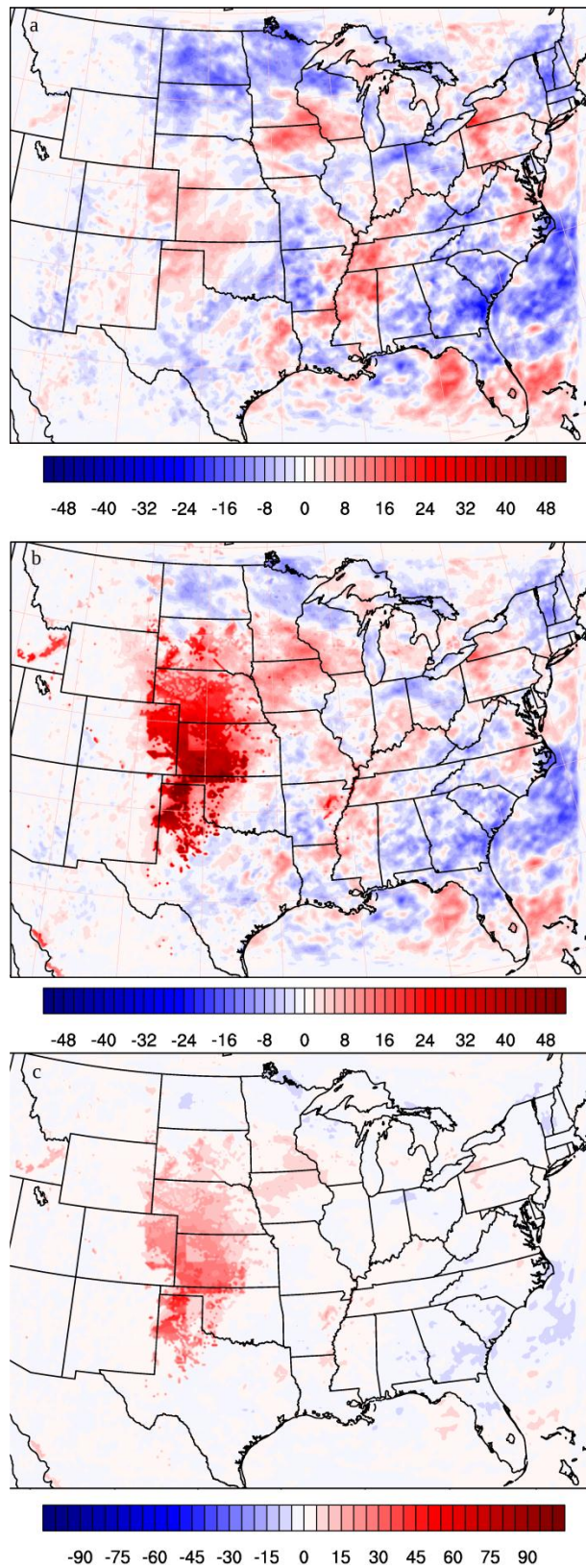
Figure 4.4 Differences in hourly averaged July (a) net shortwave and (b) net radiation (W m^{-2}), and (c) percent differences of net radiation between the Irrigated and Control cases.

western Arkansas, parts of the northeast, and the southeastern states, and decreased cloud cover over the irrigated regions, the Mississippi River Valley, northern Iowa, and some of the New England states.

As ascertained by figure 4.4b, net radiation is greater over much of the domain in the Irrigated case. The major influences of the changes in net radiation differ from region to region. Over the irrigated regions, the increase in LE, and subsequent cooling of the surface and reduction in upwelling longwave radiation, increase net radiation. More energy is therefore available at the surface to be partitioned into latent and sensible heat flux, with more energy going into latent heat flux than sensible. In the northern plains, decreased upwelling longwave radiation is partially balanced by decreased downwelling shortwave radiation, causing increased net radiation over South Dakota, and decreased net radiation over North Dakota and northern Minnesota. Elsewhere in the domain, the primary forcing affecting net radiation is the change in shortwave radiation arriving at the surface.

4.3   Thermodynamics of the Atmosphere

This section discusses the impacts of irrigation on the thermodynamic properties of the atmosphere at three points (Figure 3.1) which exemplify three different effects that irrigation has on convective potential. The first point (I) is located in southwest Kansas, surrounded completely by irrigated agriculture. Point II's location is in northwest Kansas, residing in a region also surrounded by irrigated agriculture, but overtop of a collection of cells containing non-irrigated agriculture. Finally, point III is located to the north and south of irrigated agriculture, overlying grass and non-irrigated cropland.

Figure 4.5a and b show the Irrigated and Control morning (1500 UTC) and evening (2200 UTC) soundings, respectively, averaged over the month of July. The lifted surface parcel is also shown in the figures for Irrigated and Control. The capping inversion in the morning soundings is slightly lower in Irrigated (~ 850 mb) than in Control (~830 mb), with potential temperatures of Control cap about 2°C higher in the Control. The surface temperatures, however, are markedly different, with surface temperatures ~6°C cooler in Irrigated. Even though the temperature of the capping inversion is lower for Irrigated, the cooler surface temperatures prevent the cap from being eroded enough for convection to occur. Though the afternoon LCL and LFC in Irrigated is nearly 100 mb lower than the Control on the average, the CIN is still considerably higher. The surface dewpoint would need to be increased another 10°C over the mean in the evening in order for the parcel to be able to rise above the capping inversion without traveling through the negative thermal energy therein.

Figure 4.6a and b show the same Skew-T log-P charts as those in 4.5a and b, except for point II. The morning soundings are quite similar in effect to those belonging to point I in reference to the capping inversion and surface dewpoint temperatures. The only major difference is that the change in surface temperatures between the Irrigated and Control soundings are nearly the same as the temperature differences of the capping inversions. However, in the evening sounding it is apparent that the similarities in the morning sounding do not result in a similar outcome in the evening. The boundary layer height of the Irrigated case is about 50 mb deeper at point II than at point I, since H values at point II are higher than point I. The higher H values also help to weaken the capping inversion. Even though the average CIN is higher in the Irrigated case at point
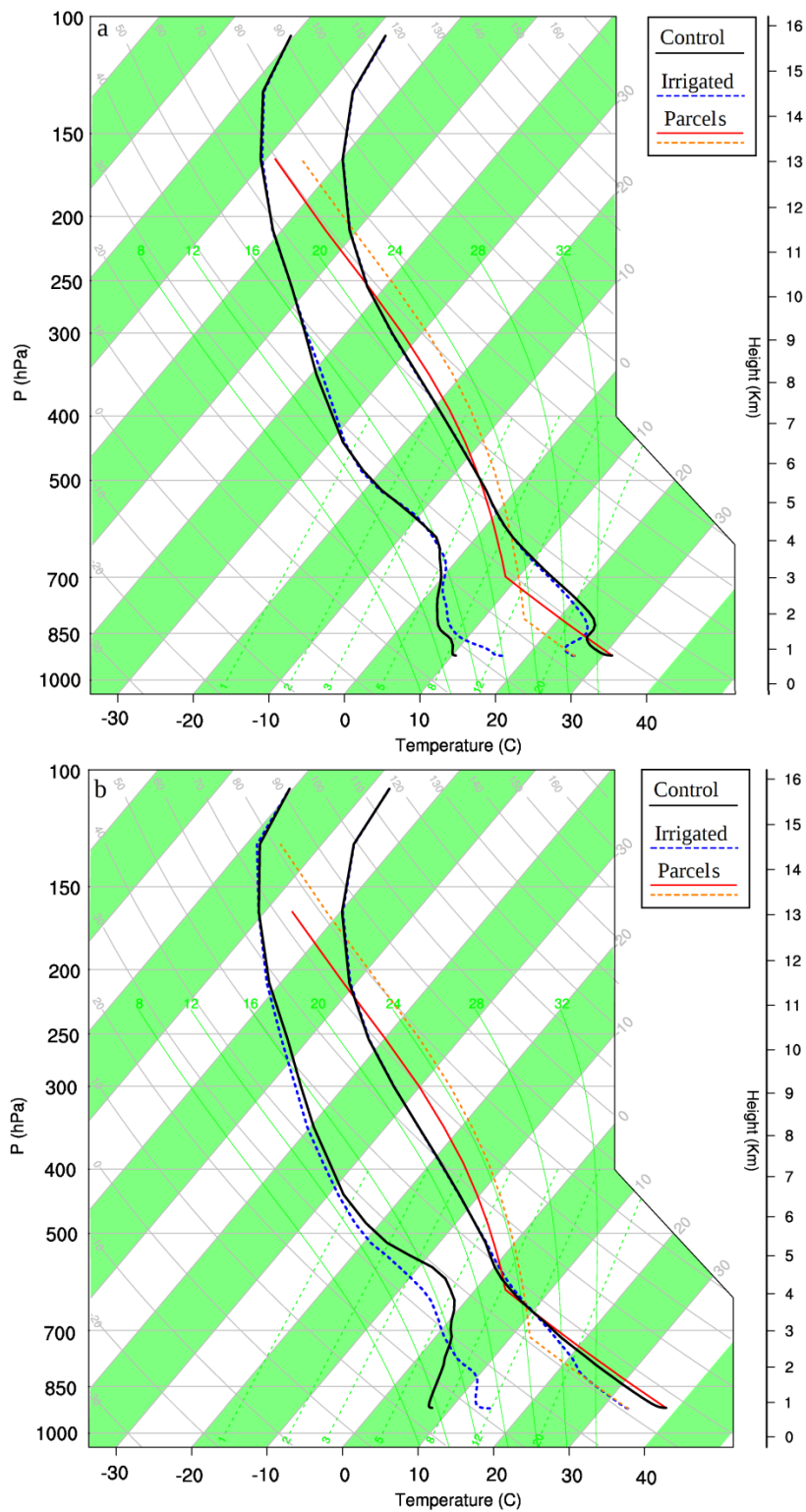
Figure 4.5 Skew-T log-P thermodynamic diagrams for location I as shown on Figure 3.1 generated from the July average conditions at (a) 1500 UTC and (b) 2200 UTC. The Control temperature and dew point temperature are denoted by solid black lines, while the Irrigated temperature and dew point temperatures are depicted by dashed blue lines. The Control parcel is represented by a solid red line, and the Irrigated parcel by a dashed orange line.

II, the CAPE is much higher, indicating that precipitation events are less likely to occur but will produce higher precipitation rates if they do.

Figures 4.7a and b are identical to Figures 4.5 and 4.6, except representing point III. As at point II, the morning sounding for point III has approximately an equal temperature difference in the surface and capping inversion temperatures. However, the height of the capping inversion in the Irrigated case is only slightly lower than the Control case for point III. Once again, the surface and boundary layer moisture profile for the morning sounding are higher in the Irrigated case, lowering the LCL and LFC throughout the day. The evening sounding for point III shows that the increase in surface MSE also increases the θ_e of the lifted parcel. Since the temperature structure of the boundary layer and capping inversion are the same in both cases, the increased θ_e has the effect of decreasing CIN because the Irrigated lifted parcel is warmer as it passes through the capping stable layer. Moreover, the higher Irrigated θ_e is associated with an increase in CAPE of nearly 60%. This indicates that Irrigated convection at point III occurs more often, and is more likely to be severe, than in Control.

4.4 Lower Atmospheric Flow

In Figure 4.8, the hourly-averaged wind velocities, geopotential height differences, and percent difference in wind speed at the 850 mb level are shown for the Irrigated and Control cases. The majority of the changes in velocity and speed are to the west and east of the irrigated regions in Kansas, Missouri, Oklahoma, Nebraska and Texas, while the largest changes in wind direction are located to the north of the irrigated regions in Nebraska and South Dakota. The exit region of the GPLLJ, located near the Nebraska-South Dakota border, is associated with convergence and upward vertical motion.
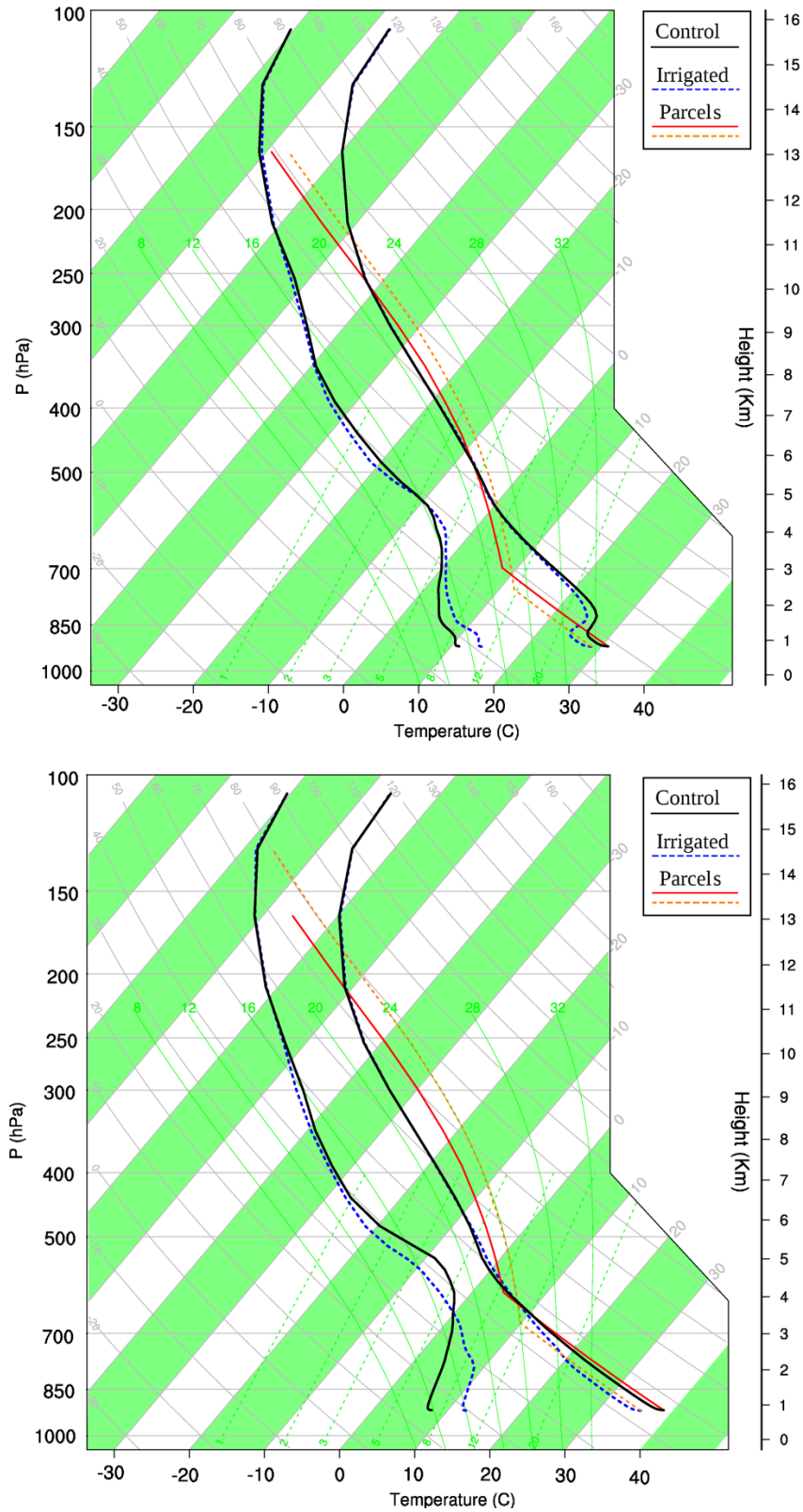
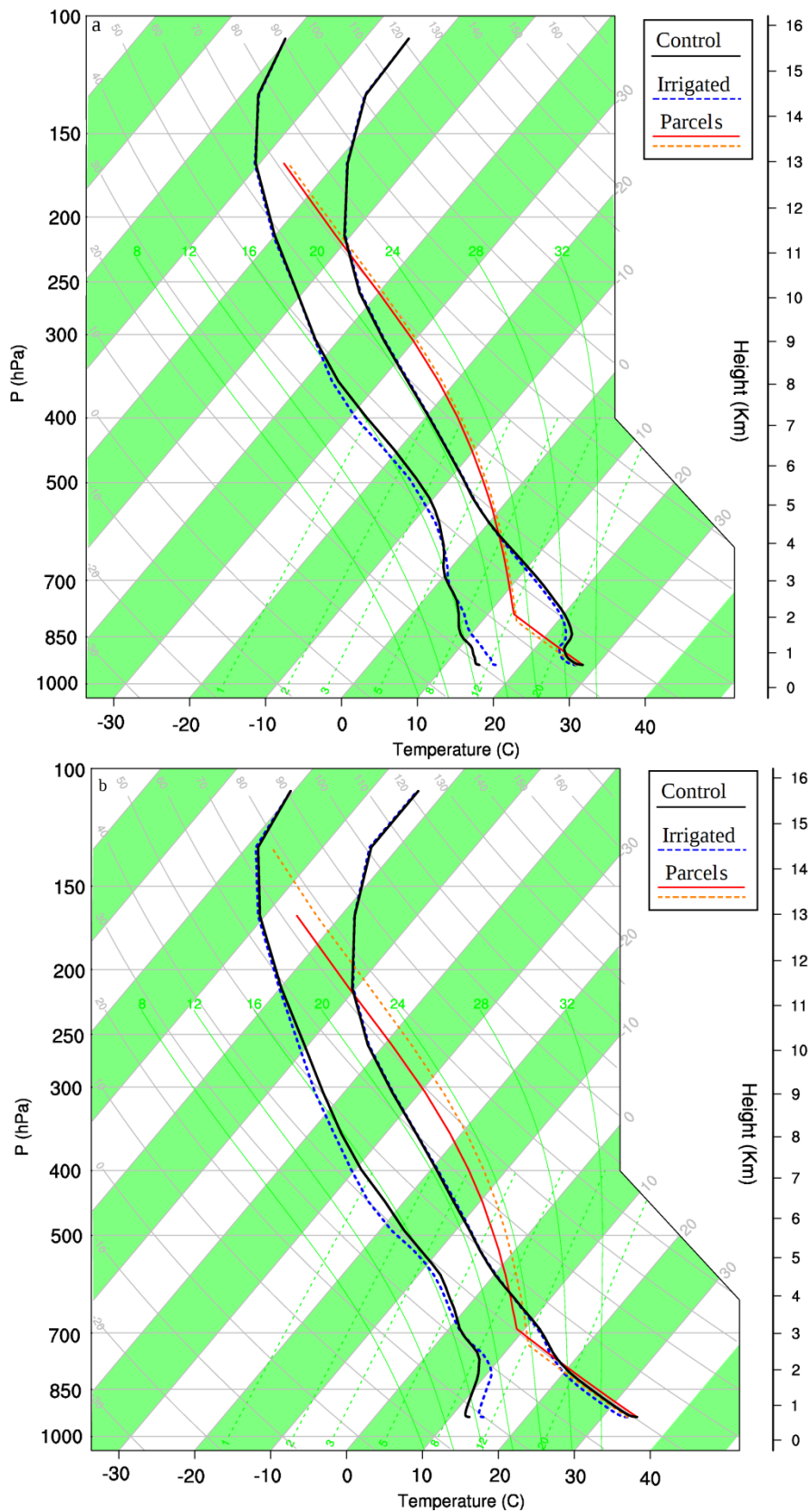**Figure 4.6** Same as Figure 4.5 except for location II as shown in Figure 3.1.

Figure 4.7 Same as Figure 4.5 except for location III as shown in Figure 3.1.

These changes are driven by the positive height anomalies over the irrigated region of the Great Plains. The decreased vertical velocities lead to less outflow near the boundary layer top, causing mass to build up in the lower portions of the atmosphere and increasing surface pressure. This increase in surface pressure forces heights upward in the lower atmosphere, as shown in Figure 4.8. To the south and east of region 1 (i.e. southeast Oklahoma, northwest Arkansas, eastern and central Texas, and southern Missouri), increased low level convergence is evinced by the differential 850 mb wind speed velocities along the flow field.
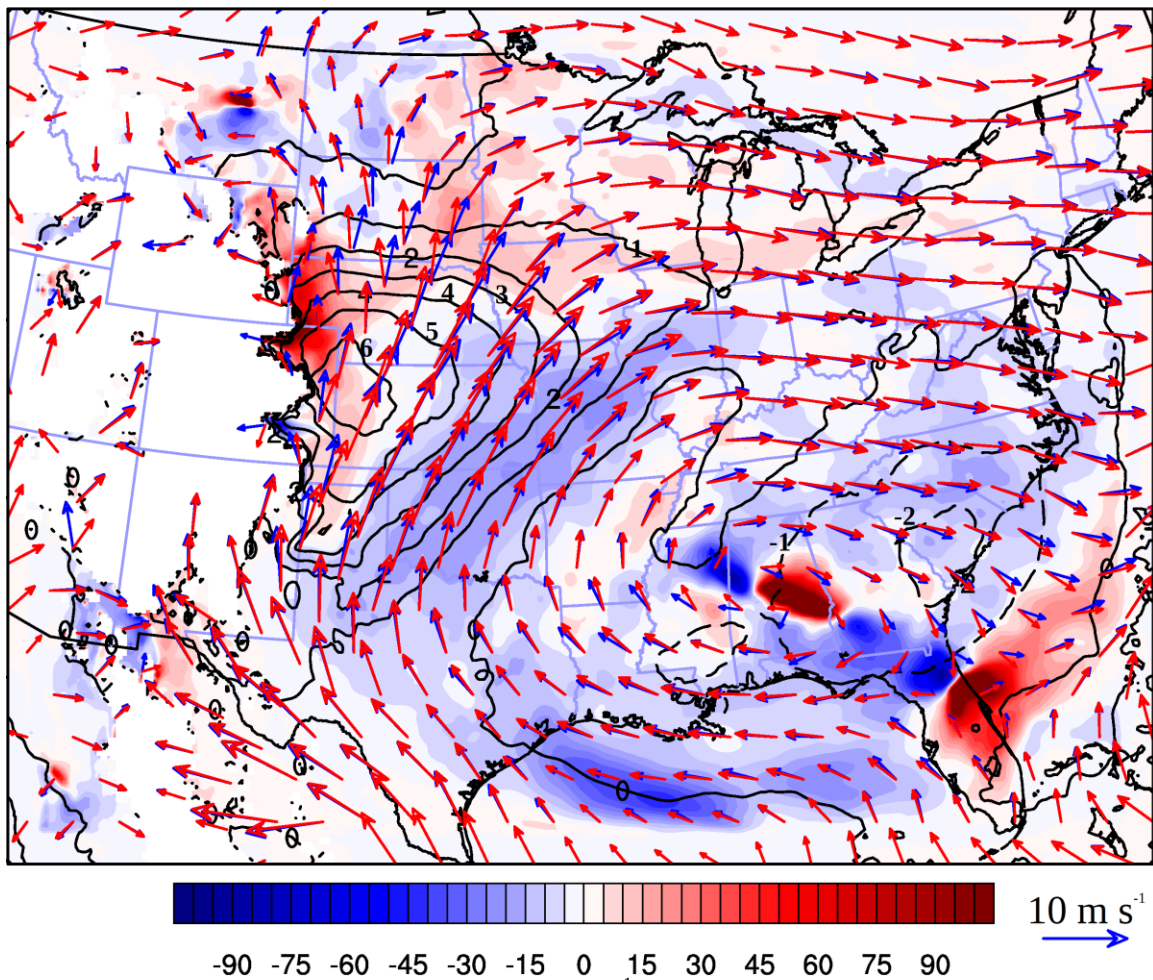
Figure 4.8 July hourly averaged 850 mb winds (m s^{-1}) Irrigated (blue vectors) and Control (red vectors) with percentage differences in wind magnitudes shown in color shaded contours. The monthly mean difference in 850 mb heights (m), calculated as the average heights of the Irrigated case minus the Control, are shown as black contours.

Figure 4.9 shows the hourly-averaged differences between Irrigated and Control 700 mb vertical velocities. At the edge of the irrigated regions, especially in north Texas, mesoscale circulations are apparent by the strong gradient of vertical velocities, with negative differences over the irrigated regions and positive just outside. The irrigated region itself is associated with enhanced downward vertical motion and divergence at low levels.

Figures 4.10a-c show the cross-sectional winds and wind differences for various time ranges over the region displayed in Figure 3.1a. The most noticeable differences occur during the day over the area just south of the irrigated region of north Texas. This region's temperature and H contrasts are the greatest between Irrigated and Control, and indicate the presence of a circulation from the cool, moist layers overlying the irrigated region to the drier, warmer regions to the south. It is apparent when comparing the differences that multiple mesoscale circulations develop during the day due to the high contrast in z_i and H. Also notable in these cross-sections is the apparent tendency for more descending winds over the Irrigated case versus the Control. The alteration to the magnitude and direction of the winds can influence the transport of many other atmospheric quantities, including water vapor.

Precipitable water (W, in mm) is defined in this study as

$$W = -\frac{1}{\rho_w g} \int_{p_{sfc}}^{\tilde{p}} q_i dp \qquad (4.2)$$

where ρ_w is the density of liquid water (kg m^{-3}), g is the acceleration due to gravity (m s^{-2}), p is pressure (kg m^{-1} s^{-2}), p_{sfc} is the pressure at the surface, $\tilde{p}$ is the pressure at the top of the model (50 mb), and q_i is the water vapor mixing ratio

(kg kg^{-1}) at the ith level of integration. The difference in hourly-averaged precipitable

water is shown in Figure 4.11a, with the percentage difference in precipitable water

represented in Figure 4.11b between the Irrigated and Control cases. Figure 4.12 shows

differences in column-integrated moisture advection. Precipitable water (W) is increased

via the introduction of water vapor from irrigation as well as the altered wind profiles.

The majority of the change in moisture throughout the domain is ~2.5 mm (~10%) and

located in the boundary layer of the Great Plains. Most of the water vapor indicated in

Figure 4.11 stays within the boundary layer until it can be transported
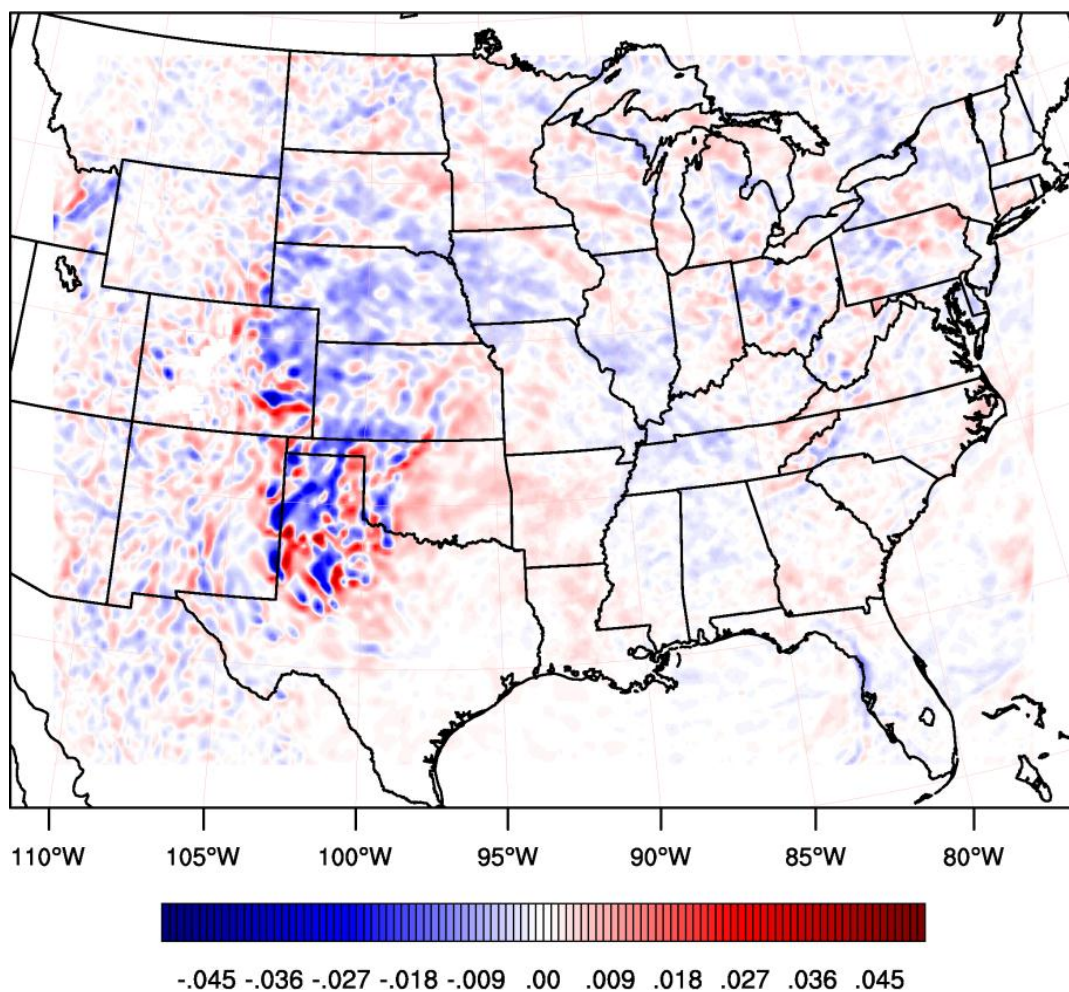
Figure 4.8 Hourly averaged differences between mean monthly 700 mb vertical velocities between the Irrigated and Control cases for the month of July (m s^{-1}).
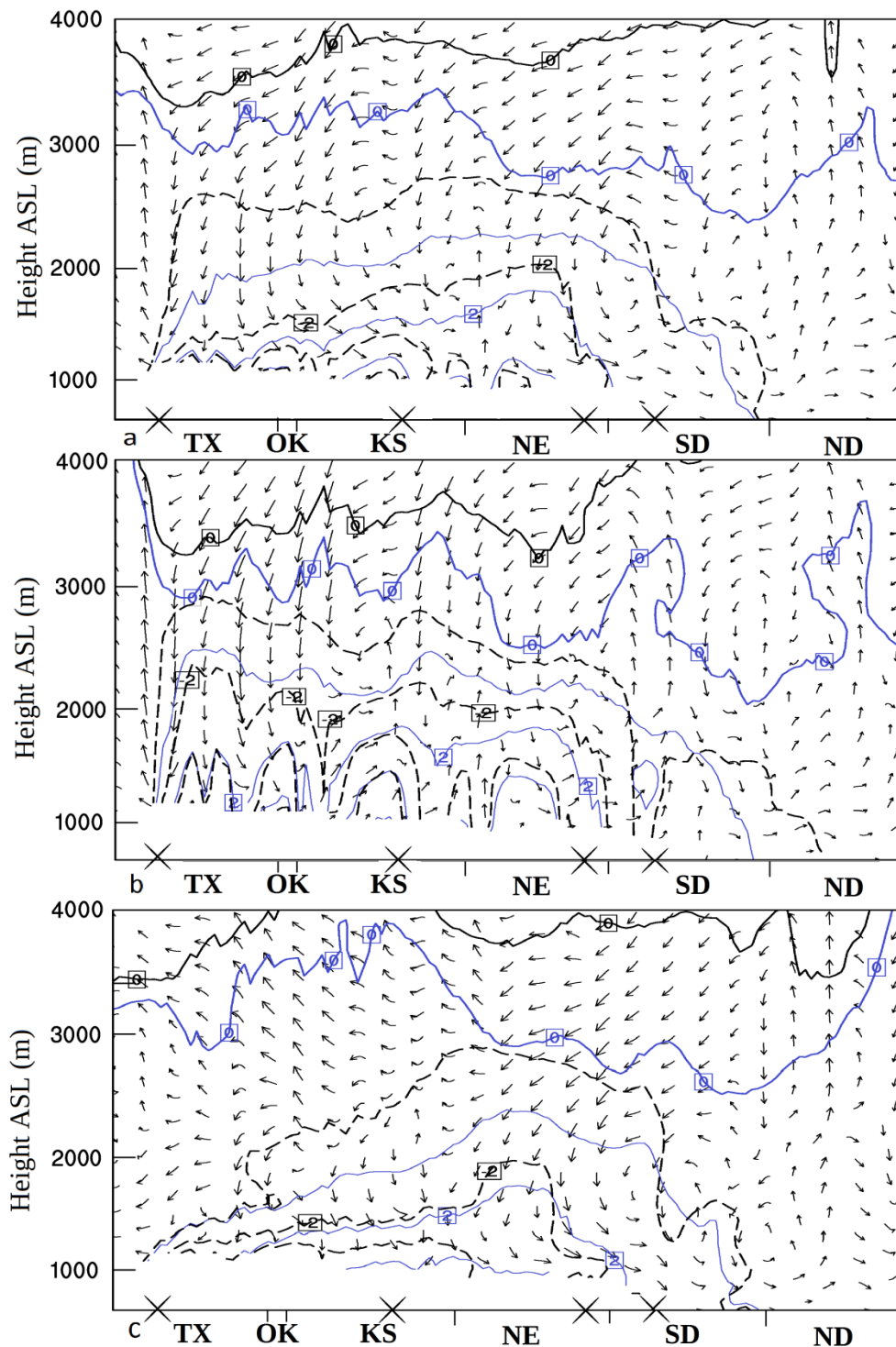
Figure 4.9 Cross-sections of hourly averaged lower atmospheric potential temperature (black contours, K), flow along the cross-section (vectors, m s⁻¹), and mixing ration (grey contours, g kg⁻¹) averaged over July and differenced between the Irrigated and Control cases for (a) the entire period, (b) the daytime hours (1800 UTC to 0000 UTC), and (c) the overnight period (0600 UTC to 1200 UTC). Crosses in a-c identify major points of land cover heterogeneity as identified in Figure 3.1. From left to right, the cross section extends from northern Texas to northeast North Dakota. Xs identify regions of heterogeneities between irrigated and non-irrigated land covers.
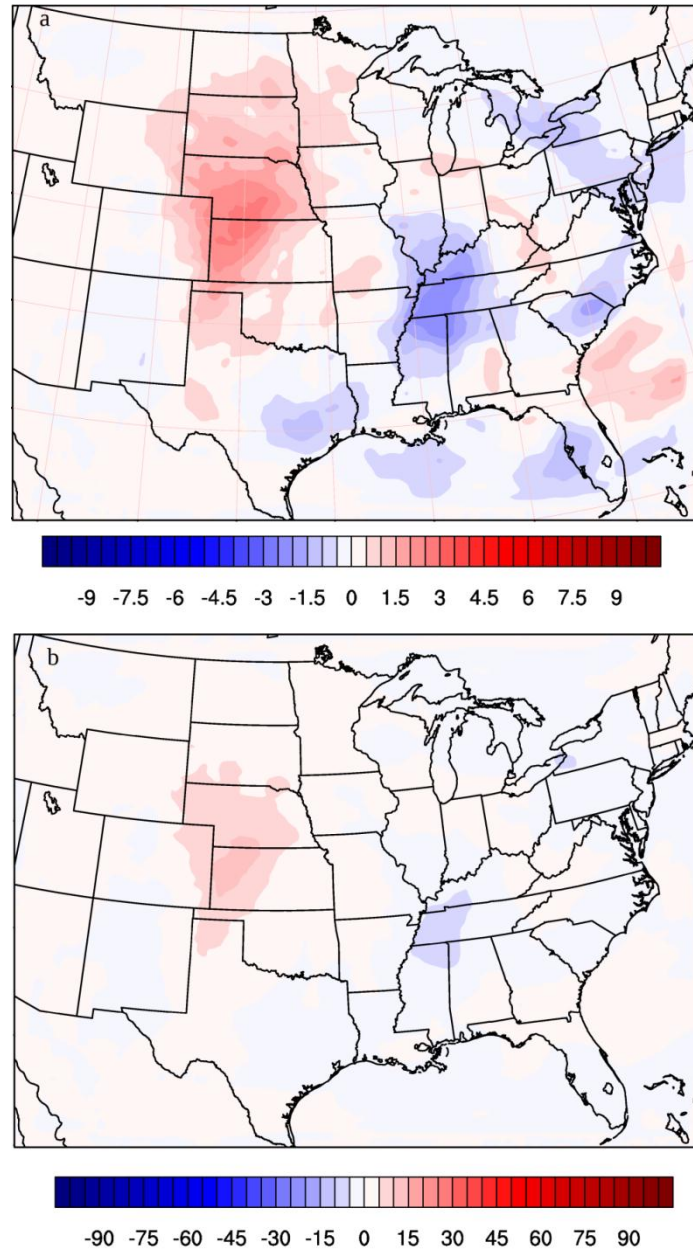
Figure 4.11 Hourly averaged (a) absolute (mm) and (b) percentage differences in precipitable water for July between the Irrigated and Control cases.

vertically by convective updrafts. From Figure 4.10, it is noticeable that moisture in the

atmosphere increases over the irrigated regions and downstream of these areas in the

vicinity of the Dakotas and Minnesota. This is caused by increased evaporation over the

irrigated areas and the transport of the moister boundary layer air to the regions

immediately downstream. In the southeast — specifically, over Kentucky, Mississippi,

Alabama, Tennessee, and South Carolina — a comparable decrease in moisture is apparent. This area is partially associated with decreased moisture advection into and increased advection out of the region as well as a slight northwestern displacement and intensification of the 850 mb high in Irrigated (Figure 4.8), which is located directly overtop the region in Control. Additionally, this area was one of the only locations to see a negative precipitation anomaly for Irrigated during the month of June (not shown), which decreased evapotranspiration rates throughout July (Figure 4.1a).
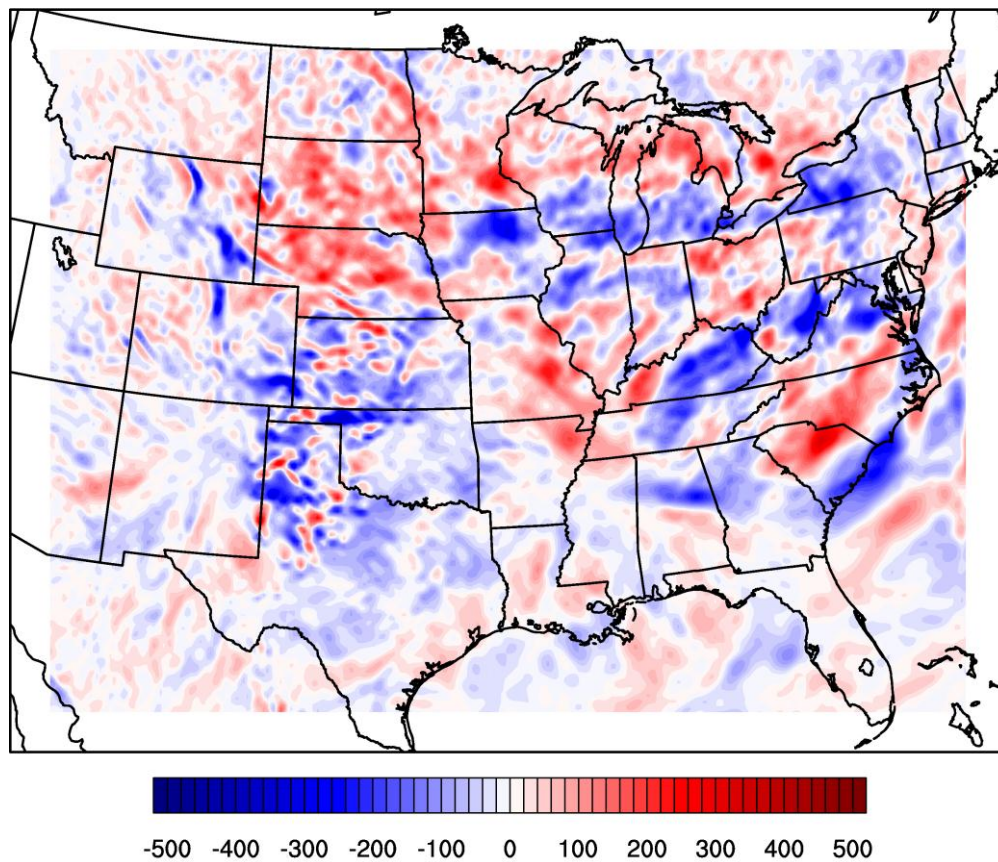
Figure 4.12 Hourly averaged differences between Irrigated and Control integrated moisture advection for the month of July(kg m^{-2} d^{-1}).

Although the winds over much of the domain are weakened, the amount of water vapor and thus the horizontal moisture gradient in the atmosphere, is increased. The increased moisture gradient between the irrigated regions and the areas downstream

increases moisture advection downwind of region 1 (Figure 4.12). However, to the south of the irrigated areas, it is evident that the slower wind speeds result in less moisture transport from the Gulf of Mexico.

4.5   Precipitation

Figures 4.13 a-d show the July accumulated precipitation for the Irrigated case, the Control case, the absolute difference between the two, and the percent difference, respectively. The changes to the radiation balance, water budget, and atmospheric flow result in changes to the precipitation patterns and intensity throughout the eastern two-thirds of the domain. The alterations to precipitation also have effects on the radiation balance and water budgets, especially in regions outside of the irrigated land use areas. Note the large (~100 mm, 100%) increase in precipitation downwind of the irrigated regions. This increase in precipitation is associated with the positive moisture advection anomalies into the region from region 1. It is apparent from these figures (in combination with Figure 4.8, showing the 850-mb flow pattern) that the majority of the differences in precipitation occur in the region just downwind of the irrigated region (the Dakotas, Minnesota, Iowa, and Michigan) and to the southeast of regions 1 and 2.

Figures 4.14a and b show the surface-based differences between Irrigated and Control CAPE and CIN, respectively, for the domain, averaged hourly over the month of July. The increase in MSE over the irrigated region causes higher values of CAPE over the same region as well as downstream into the Dakotas and southwestern Minnesota. The increase in CIN over the irrigated region is associated with weakened boundary layer thermals produced by a decrease in sensible heat in the region.
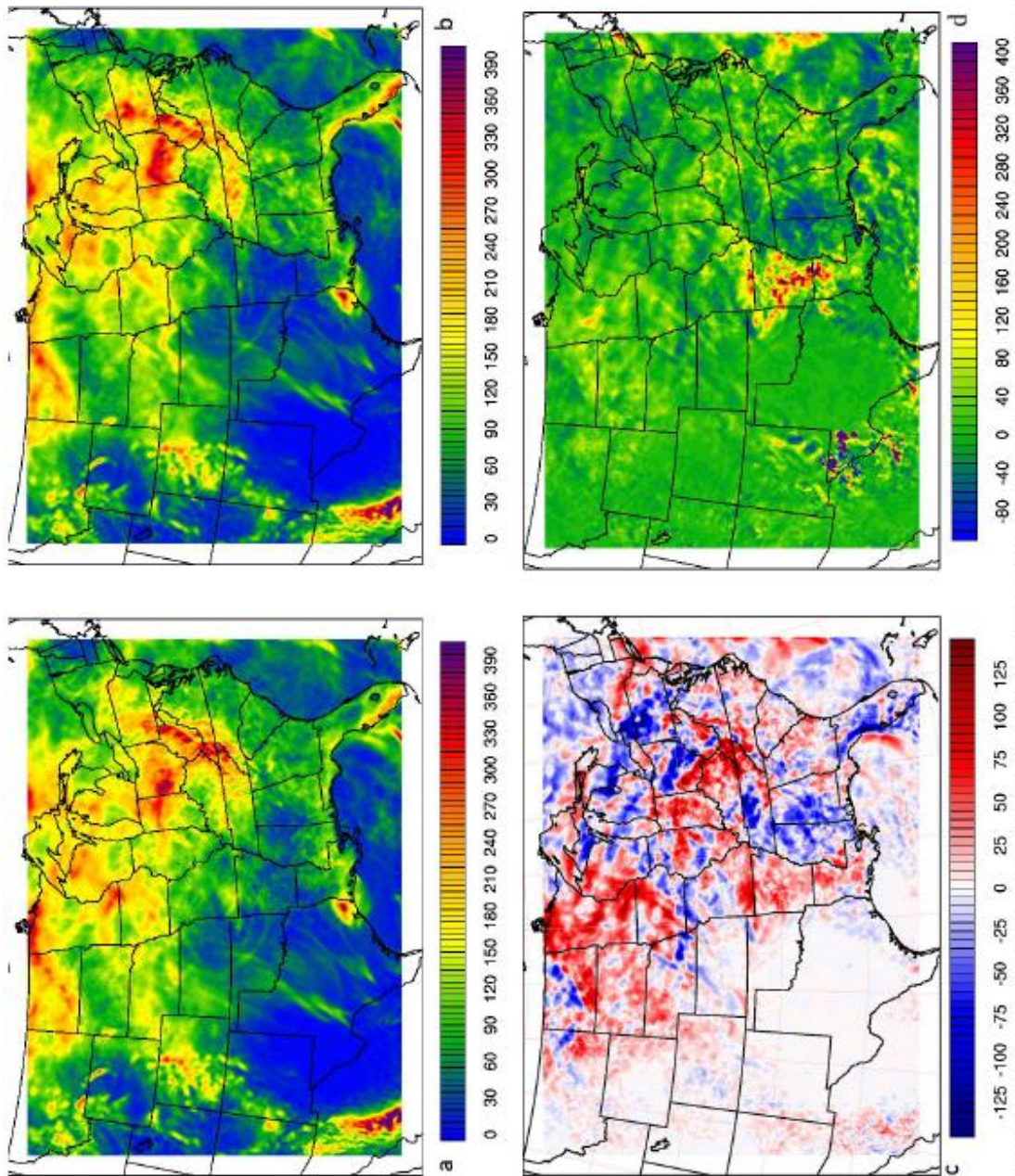
Figure 4.15 Total precipitation (mm) summed over the month of July for the (a) Irrigated and (b) Control cases and (c) the absolute and (d) percent differences between the two.

Also being advected into the region east of the irrigation (Iowa, Missouri, Arkansas, Illinois, and Mississippi) are cooler surface to 700 mb temperatures (not shown). The air at 700 mb is cooled more than the air at the surface is through this region, so the environmental lapse rates in these areas are increased while also increasing moisture
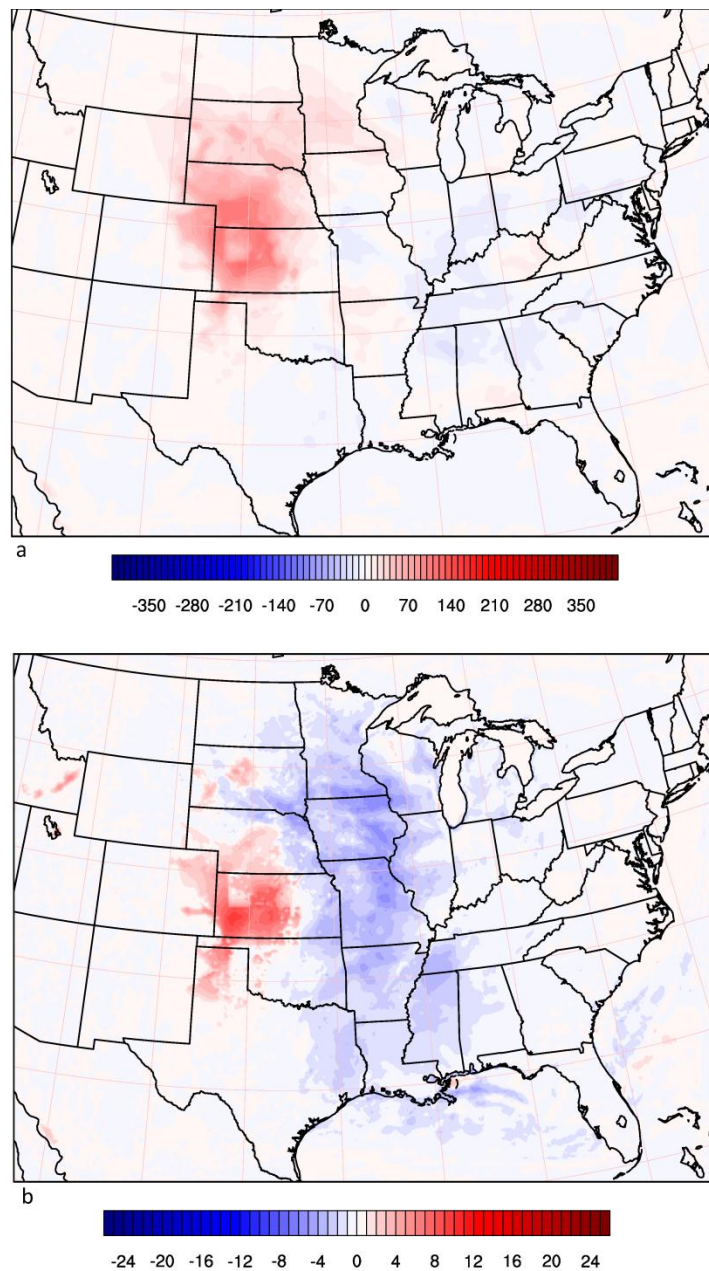
Figure 4.15 Hourly averaged differences for the month of July for (a) CAPE (J kg^{-1}) and (b) CIN (J kg^{-1}) between Irrigated and Control cases.

profiles (see section 4.3). This increase in lapse rates is responsible for decreasing the CIN throughout this region. To the southeast of the irrigated region, decreased temperature advection associated with a weaker low level jet reduces temperatures around the 700 mb level more so than at the surface, establishing a similar increase in low level lapse rates and decreasing the CIN in the region.

Immediately to the north of the irrigated region, a zonal strip of decreased CIN is also evident. This decrease in CIN is associated with increased low level convergence at the exit region of the GPLLJ. This area also experiences an increase in precipitation, which could be responsible for the increase in convergence into the region as well. The low-level convergence in the region forces boundary layer air to rise and more quickly erode the capping inversion than in a non-convergent flow scheme, thusly decreasing the CIN. The increase in CAPE and simultaneous decrease in CIN over northern Nebraska, southern South Dakota, and southern Minnesota leads higher precipitation totals and greater probabilities of individual precipitation events being severe.

4.6   Subdomain Analyses

The averaged components of the radiation balance for regions 1 and 2, as indicated in Figure 3.1a, are shown in Table 4.1. In both regions, the predominant alterations to the radiation balance occur at the repartitioning of the latent and sensible heat fluxes. Over region 1, the net radiation increases by over 20%, which is attributable to lower upwelling longwave radiation values generated from cooler temperatures at the surface. This same effect is also perceivable in the downstream region, but to a much lesser extent. The higher net longwave radiation and slightly elevated shortwave radiation in the evenings of the irrigated region promote higher surface turbulent flux emissions.

Table 4.2a shows the 2-m MSE, surface based CAPE and CIN, and 2-m temperature and mixing ratio for the subdomains pictured in Figure 3.1a. The increases in MSE are associated with the increased surface fluxes. Again, it is noticeable that the MSE is markedly higher over the irrigated region than it is downstream. This is due in part to the realization of the MSE in the downstream region through convection, but also that the energy over the irrigated region is constantly supplied by higher net radiation incident at the surface. It is interesting to note that MSE is higher due to the increase in moisture in both the irrigated and downstream regions, and the decrease in 2-m temperatures only partly balance the increased MSE associated with greater atmospheric moisture content.

Table 4.1 Alterations to the radiation balance and temperature in the two subdomains identified in Figure 4.13. Units for temperature (T) are Kelvins. For all other terms, the units are W m^{-2}.

Region 1				Region 2			
	Irrigated	Control	Difference (%)		Irrigated	Control	Difference (%)
T (K)	301.89	306.57	-4.68 (-1.52)	T (K)	299.40	300.42	-1.02 (-0.34)
H (W m^{-2})	20.55	57.59	-37.03 (-64.3)	H (W m^{-2})	34.15	39.13	-4.98 (-12.7)
LE (W m^{-2})	142.69	75.39	67.3 (89.3)	LE (W m^{-2})	111.97	101.42	10.55 (10.4)
G (W m^{-2})	-6.79	-7.27	0.48 (6.60)	G (W m^{-2})	-8.12	-8.54	0.43 (4.91)
Net Flux (W m^{-2})	156.45	125.70	30.75 (24.5)	Net Flux (W m^{-2})	138.00	132.00	6.00 (4.55)
Upwelling LW (W m^{-2})	458.05	487.98	-29.93 (-6.13)	Upwelling LW (W m^{-2})	432.72	438.74	-6.02 (-1.37)
Downwelling LW (W m^{-2})	370.84	374.99	-4.15 (-1.11)	Downwelling LW (W m^{-2})	372.86	371.91	0.95 (0.26)
Net LW (W m^{-2})	-87.20	-112.99	25.78 (22.8)	Net LW (W m^{-2})	-59.86	-66.84	6.97 (10.4)
Net SW (W m^{-2})	268.13	263.78	4.35 (1.64)	Net SW (W m^{-2})	234.17	235.95	-1.77 (-0.75)
R$_n$ (W m^{-2})	174.13	143.52	30.61 (21.3)	R$_n$ (W m^{-2})	166.20	160.57	5.63 (3.51)

The increase in 2-m MSE from increased net radiation are reflected in the increased values of CAPE and CIN for the downwind and irrigated regions. In the irrigated region, the increase in CIN over the entire diurnal period keeps the additional CAPE from being realized, and so the MSE and associated CAPE increases to values much higher than in the downwind region where CIN is decreased. The reason for the smaller increase in CAPE downstream is likely that the region more readily uses up the additional CAPE supplied to it. The increase in CIN over the irrigated region is related to the decreased

sensible heat flux, since the capping inversion is much more slowly eroded by boundary

layer convection.

Table 4.2 Comparison of thermodynamic quantities of the atmosphere between the Irrigated and Control cases over the two regions identified in Figure 15. The units for temperature and dew point temperature are K, while CAPE and CIN are in J kg^{-1}, and MSE is in kJ kg^{-1}.

| Region 1				Region 2			
	Irrigated	Control	Difference (%)		Irrigated	Control	Difference (%)
T (K)	301.89	306.57	-4.68 (-1.52)	T (K)	299.40	300.42	-1.02 (-0.34)
T_d (K)	287.51	282.61	4.90 (1.73)	T_d (K)	288.14	286.81	1.59 (0.46)
CAPE (J kg^{-1})	654.66	209.83	444.83 (212.0)	CAPE (J kg^{-1})	791.83	577.51	214.32 (37.1)
CIN (J kg^{-1})	160.65	74.90	85.75 (114.5)	CIN (J kg^{-1})	103.76	122.25	-18.49 (-15.1)
MSE (J kg^{-1})	331.56	326.66	5.01 (1.50)	MSE (J kg^{-1})	328.21	326.61	1.33 (0.49)
P (mm)	12.53	13.60	-1.07 (7.87)	P (mm)	82.73	56.85	25.88 (45.52)
E (mm)	78.01	41.22	36.79 (89.27)	E (mm)	61.22	55.45	5.77 (10.40)
P_{tot} (10^{12} kg)	2.39	2.60	-0.20 (-7.87)	P_{tot} (10^{12} kg)	39.56	27.19	12.38 (45.52)
E_{tot} (10^{12} kg)	14.90	7.87	7.02 (89.25)	E_{tot} (10^{12} kg)	29.28	26.52	2.76 (10.40)

a

	Irrigated	Control	Difference (%)
E_{irr} (10^{12} kg)	78.71	39.68	36.02 (90.77)
E_{dom} (10^{12} kg)	1267	1195	72.35 (6.05)
P_{dom} (10^{12} kg)	756.4	725.6	30.87 (4.25)

b

Figures 4.16 a-d show the time-series of precipitation over regions 1 and 2 as well as

the cumulative difference in precipitation. It is evident in both cases that the number of

events do not change, but rather the intensity of each event is responsible for the overall

accumulation differences. By the end of the month, there is over a 2.5-cm average

increase in precipitation in the region downstream of the irrigated agriculture. This

difference is due to the increase in moisture in the atmosphere and increased fluxes at the

surface leading to higher values of CAPE and MSE. For the irrigated region, the change

in precipitation is slightly negative, though negligible, due to the low number of

convective events occurring in the area.
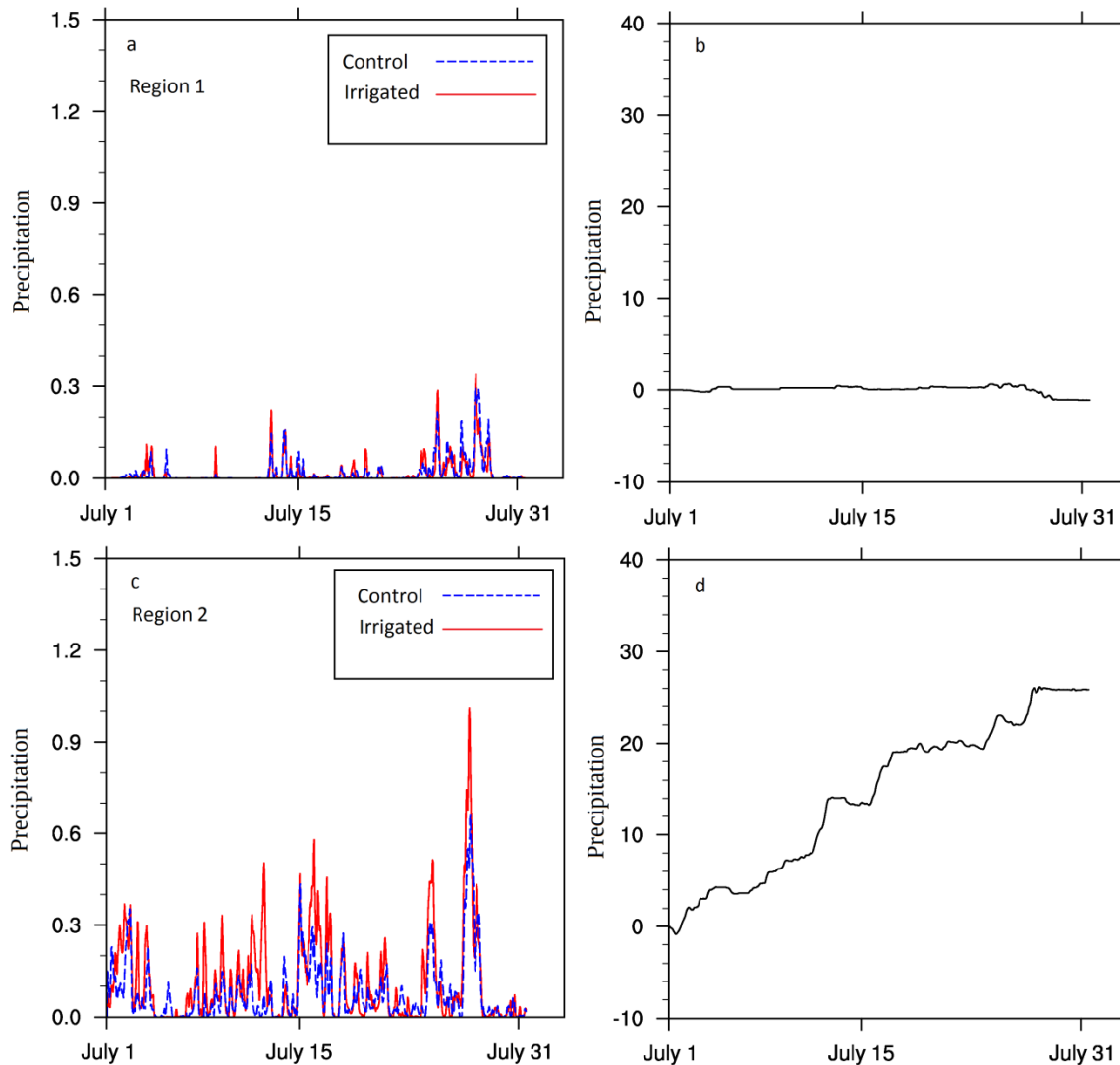
Figure 4.16 Precipitation (mm) time-series for irrigated (a and b), and downwind (c and d) regions of the domain as shown in Figure 15. Figures a and c show Irrigated and Control hourly accumulations, while Figures b and d display accumulation differences.

The accumulated difference in precipitation in region 2 cannot be fully explained by the extra evaporation from region 1 since the change in mass of evaporated water between the Irrigated and Control cases over region 1 is less than the change in precipitation over region 2. Table 4.2b shows the domain summed differences in evaporation over irrigated cells (E_{irr}) and the entire domain (E_{dom}) as well as the summed differences in precipitation over the domain (P_{dom}). The change in precipitation over region 2 is only about a third of E_{irr}, while the total increase in precipitation over the

entire domain accounts for 85.71% of increase in evaporated water from irrigated

locations and the change in P_{dom} accounts for only 42.67% of the increase in E_{dom}. The

rest of the evaporated water over the entire domain either remains in the atmosphere as

water vapor, cloud ice, or cloud water, or it is transported out of the domain.

Chapter 5

Discussion and Conclusions

5.1   Discussion of Results

The results presented here demonstrate the capability of irrigation to drastically alter the

flow, moisture, and radiation regimes. These alterations result in different patterns of

precipitation which in turn also affect regimes further downstream of the original increase

in soil moisture. The cooling of the lower atmosphere from evaporation has the ability to

regionally mask the temperature change due to increased global greenhouse gasses, and

may even cool the surface enough locally that the temperatures over irrigated regions

have decreased. This is in agreement with many other studies investigating the effects of

irrigation on temperature and the radiation balance (e.g. Adegoke et al. 2003; Kueppers et

al. 2007; Suyker and Verma, 2009; and Puma and Cook, 2010). Therefore, the results

found for the present study suggest that irrigation is a first-order climate forcing on the

regional scale with respect to temperature (Hansen et al., 2005). Additionally, as

discussed by Brunsell et al. (2010), the amount of heating expected due to the increase of

greenhouse gasses (IPCC, 2007) may not as strongly influence regions like the western Great Plains.

Other noteworthy impacts of irrigation are the increases to precipitation downstream, alterations to the local and regional flow, and changes to the radiation balance. These impacts, with some notable exceptions to precipitation (e.g. Barnston and Schickedanz, 1984; and Moore and Rojstaczer, 2002) have not received nearly as much attention as effects on surface temperature. The forcing exerted on the climate by evapotranspiration from irrigated water to cool the lower portions of the atmosphere is an important one, but the alterations to the radiation budget caused by this make it a significant climate forcing, especially when considering effects beyond temperature.

The preferential cooling of the surface and boundary layers associated with evapotranspiration over irrigated regions while not affecting regions upstream of the irrigated lands alters the pressure and height patterns of the surface and lower atmosphere, thusly altering flow patterns in and around irrigated agriculture. This impact on flow magnitude has major implications when considering the alternative power source of wind energy. In this study, the addition of irrigation results in decreased wind speeds throughout most of Kansas, a state in which wind energy is beginning to flourish. The irrigated region itself is associated with enhanced downward vertical motion and divergence at low levels. The use of irrigation disconcerting to those who might benefit from this renewable energy source.

Increases in MSE resulting from cooler temperatures and higher water vapor mixing ratios over the irrigated and downstream land masses result in high CAPE values over the same regions, as well as those downstream. Higher sensible heat fluxes downwind of the

irrigated zones then create more turbulent boundary layers which can mix out the capping inversion. The erosion of the capping inversion eventually leads to situations where deep convective updrafts can transport the excessive moisture from the boundary layer and generate intense precipitation. As shown previously in Figures 4.16a and b, the number of precipitation events does not seem to change much downstream, though the amount of precipitation per event does increase. This, coupled with the higher CAPE values, implies that precipitation events are more likely to be severe and likely produce more flood and flashflood incidents. This is in agreement with the observational study of river discharge rates by Kustu et al. (2011).
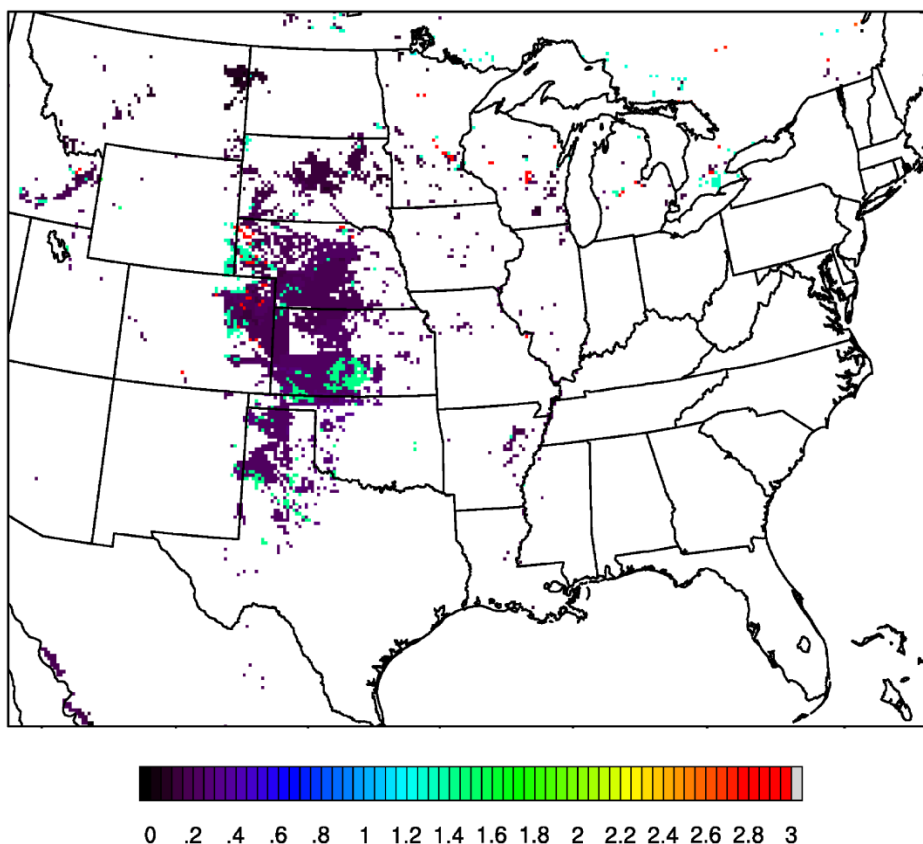
Figure 5.1 Total water applied to irrigated grid cells over the month of July in Irrigated (m).

When the Ogallala aquifer is no longer a viable source of water for irrigation, not only will the primary source of drinking water for much of the Great Plains also be

depleted, but the extra sources of water vapor will also decrease throughout North America. This will result in decreased precipitation in many regions of the United States, including the northern Great Plains which has experienced higher precipitation amounts over much of the past 40 years. This will also have the effect of decreasing stream flow of the major river systems of North America, which will increase river pollution since the concentration of pollutants will increase, and also make the renewable energy source of hydroelectric more difficult to use effectively.

Although this set of simulations has demonstrated many of the forcing and feedback mechanisms that irrigation is capable of producing, it is important to note that this is a sensitivity study, and that the results from either simulation presented within this paper are not intended to match observations from the Summer of 2001 in the U.S. or any other period over the U.S. or any other region.

The total water applied in the Irrigated case is shown in Figure 5.1b. The majority of the irrigated grid cells received between 0.05 and 0.3 m of water over the period. The amount of irrigation that these grid cells received is extremely high, as the typical amount applied over an entire growing season (mid-May to mid-October) ranges from 0.2 to 0.3 m for corn and just about 0.2 m for soy beans, with significant amounts of water still being applied in August and September (Suyker and Verma, 2009).

5.2   Conclusion

The increase in soil moisture from irrigation provides a strong forcing for alterations to the radiation balance and water budget which results in changes in flow, atmospheric water content and transport, precipitation, and temperature over much of the United States. All of the changes examined in this paper have stemmed from the excessive

evaporation caused by simulated irrigation in the Great Plains. Enhanced evaporation increases latent heat flux and decreases sensible heat flux which drives temperatures over irrigated areas lower. Cooler temperatures over the irrigated areas contrasted to the warmer land surrounding them set up circulations similar to a land-sea breeze that causes divergence (convergence) values to decrease (increase) and descending momentum over the irrigated areas. Descending vertical motion coupled with lower sensible heat release over the irrigated region causes CIN values to increase, and while increased net radiation increases CAPE values over the same area, the increased CIN caps the boundary layer too strongly for this energy to be realized, causing fewer (but stronger) precipitation events to occur over the irrigated region.

Regions downwind of irrigation are influenced by advection of cooler, moister, and more energetic (larger values of MSE) air. The results show that there is an increase in CAPE due to the increase in energy in the boundary layer and slight decrease in CIN associated with higher sensible heat release. The more energetic, moist, and convectively prone boundary layer leads to greater precipitation amounts downstream of the irrigated region, though the number of events does not change. Irrigation results in a change in 850-mb height patterns, causing the prevailing winds to alter direction from southwest to south at the 850 mb level, thus increasing veering in the lower atmosphere, causing more severe convection to take place in the northern Plains states.

The effects discussed in this paper outline the dramatic capabilities of anthropogenic land cover change to alter the climate. Land cover change has been overlooked by much of the climate community as a mechanism for altering the weather patterns, even though it has been shown to be a first-order forcing at the regional scale (Pielke, 2005). The

ability of water vapor introduced in mass quantities through irrigation proves to be a significant source of climate change in regions such as the Great Plains, where mid-summer convection is enhanced by excessive moisture and potential energy. This shows that research should continue on regional land cover change to identify the effects of anthropogenic introductions of moisture and energy into the atmosphere at the regional and global scales.

Bibliography

Adegoke, J. O., R. A. Pielke, J. Eastman, R. Mahmood, and K. G. Hubbard, 2003: Impact of irrigation on midsummer surface fluxes and temperature under dry synoptic conditions: A regional atmospheric model study of the U.S. High Plains. *Mon. Wea. Rev.,* **131**, 556-564.

Anderson, J. R., E. E. Hardy, J. T. Roach, and R. E. Witmer, 1976: A Land Use and Land Cover Classification System for use with Remote Sensor Data. U.S. Geological Survey Professional Paper 964, U.S. Geological Survey, Reston, VA, USA.

Arnfield, A., 2003: Two decades of urban climate research: A review of turbulence, exchanges of energy and water, and the urban heat island. *Int. J. Climatol.,* **23**, 1-26.

Arritt, R. W., T. D. Rink, M. Segal, D. P. Todey, C. A. Clark, M. J. Mitchell, and K. M. Labas, 1997: The Great Plains low-level jet during the warm season of 1993. *Mon. Wea. Rev.,* **125**, 2176-2192.

Avissar, R., and Y. Liu, 1996: Three-dimensional numerical study of shallow convective clouds and precipitation induced by land surface forcing. *J. Geophys. Res.,* **101**, 7499-7518.

Barnston, A. G., and P. T. Schickedanz, 1984: The effect of irrigation on warm season

   precipitation in the southern Great Plains. *J. Climate Appl. Meteor.*, **23**, 865-888.

Betts, A. K., J. H. Ball, A. C. Beljaars, M. J. Miller, and P. Viterbo, Coupling between

   land-surface, boundary-layer parameterizations and rainfall on local and regional

   scales: Lessons from the wet summer of 1993, paper presented at Fifth Conference on

   Global Change Studies, Am. Meteorol. Soc., Nashville, Tenn., 1994.

Black, T. L., 1994: The new NMC mesoscale Eta model: Description and forecast

   examples. *Wea. Forecasting,* **9**, 265-278.

Boucher, O., G. Myhre, and A. Myhre, 2004: Direct human influence of irrigation on

   atmospheric water vapour and climate. *Clim. Dyn.,* **22**, 597-603.

Brunsell, N. A., A. R. Jones, T. L. Jackson, J. J. Feddema, 2010: Season trends in air

   temperature and precipitation in IPCC AR4 GCM output for Kansas, USA: evaluation

   and implications. *Int. J. Climatol.*, **30**, 1178-1193.

Bryan, G. H., J. C. Wyngaard, and J. M. Fritsch, 2003: Resolution requirements for the

   simulation of deep moist convection. *Mon. Wea. Rev.,* **131**, 735-744.

Chen, F. and J. Dudhia, 2001: Coupling an advanced land surface–hydrology model with

   the Penn State–NCAR MM5 modeling system. Part I: Model implementation and

   sensitivity. *Mon. Wea. Rev.,* **129**, 569-585.

Clark, C. A., and R. W. Arritt, 1995: Numerical simulations of the effect of soil moisture

   and vegetation cover on the development of deep convection. *J. Appl. Meteor.,* **34**,

   2029-2045.

Cook, K. H., E. K. Vizy, Z. S. Launer, and C. M. Patricola, 2008: Springtime intensification of the Great Plains low-level jet and Midwest precipitation in GCM simulations of the twenty-first century. *J. Climate,* **21**, 6321-6340.

Deardorff, J. W., 1974: Three-dimensional numerical study of the height and mean structure of a heated planetary boundary layer. *Bound.-Layer Meteor.,* **7**, 81-106.

DeRidder, K., and H. Gallée, 1998: Land surface-induced regional climate change in southern Israel. *J. Appl. Meteor.,* **37**, 1470-1485.

Douglas, E. M., A. Beltrán-Przekurat, D. Niyoki, R. A. Pielke Sr., C. J. Vörösmarty, 2009: The impact of agricultural intensification and irrigation on land-atmosphere interactions and Indian monsoon precipitation – A mesoscale modeling perspective. *Global Planet. Change,* **67**, 117-128.

Ek, M. B., K. E. Mitchell, Y. Lin, E. Rogers, P. Grunmann, V. Koren, G. Gayno, and J. D. Tarpley, 2003: Implementation of Noah land surface model advances in the National Centers for Environmental Prediction operational mesoscale Eta model. J. Geophys. Res., 108, D22, 8851, doi:10.1029/2002JD003296.

Eltahir, E. A. B, 1998: A soil moisture-rainfall feedback mechanism 1. Theory and observations. *Water Resour. Res.,* **34**, 765-776.

Entekhabi, D., I. Rodriguez-Iturbe, F. Castelli, 1996: Mutual interaction of soil moisture state and atmospheric processes. *J. Hydrol.,* **184**, 3-17.

Findell, K. L., and E. A. B. Eltahir, 2003: Atmospheric controls on soil moisture-boundary layer interactions. Part I: framework development. *J. Hydromet.,* **4**, 552-569.

Findell, K. L., and E. A. B. Eltahir, 2003: Atmospheric controls on soil moisture-boundary layer interactions. Part II: Feedbacks within the continental United States. *J. Hydromet.,* **4**, 570-583.

Fritsch, J. M., R. J. Kane, and C. R. Chelius, 1986: The contribution of mesoscale convective weather systems to the warm-season precipitation in the United States. *J. Climate Appl. Meteor.,* **25**, 1333-1345.

Gutentag, E.D., Heimes, F.J., Krothe, N.C., Luckey, R.R., and Weeks, J.B., 1984: Geohydrology of the High Plains aquifer in parts of Colorado, Kansas, Nebraska, New Mexico, Oklahoma, South Dakota, Texas, and Wyoming: U.S. Geological Survey Professional Paper 1400–B, 63 p.

Hansen, J. and Coauthors, 2005: The efficacy of climate forcings. *J. Geophys. Res.,* **110**, D18104.

Higgins, R. W., Y. Yao, E. S. Yarosh, J. E. Janowiak and K. C. Mo, 1997: Influence of the Great Plains low-level jet on summertime precipitation and moisture transport over the central United States. *J. Climate,* **10**, 481-507.

IPCC, 2007: Climate change 2007: Impacts, adaptation and vulnerability. Cambridge University Press, Cambridge.

Jones, A. R. and N. A. Brunsell, 2008: A scaling analysis of soil moisture-precipitation interactions in a regional climate model. *Theor. Appl. Climatol.* **98**, 221-235.

Kueppers, L. M., M. A. Snyder, and L. C. Sloan, 2007: Irrigation cooling effect: regional climate forcing by land-use change. *Geophys. Res. Lett.,* **34**, L03703.

Kustu, M. D., Y. Fan, and M. Rodell, 2011: Possible link between irrigation in the U.S. High Plains and increased summer streamflow in the Midwest. *Water Resour. Res.*, **47**, W03522.

Lohar, D., and B. Pal, 1995: The effect of irrigation on premonsoon season precipitation over south west Bengal, India. *J. Climate*, **8**, 2567-2570.

Margulis, S. A., D. McLaughlin, D. Entekhabi, and S. Dunne, 2002: Land data assimilation and soil moisture estimation using measurements from the southern Great Plains 1997 field experiment. *Water Resour. Res.,* **38,** 1299, doi:10.1029.

Maxwell, R. M., F. K. Chow, and S. J. Kollet, 2007: The groundwater-land-surface-atmosphere connection: Soil moisture effects on the atmospheric boundary layer in fully-coupled simulations. *Adv. Water Resour.*, **30**, 2447-2466.

McGuire VL, Johnson MR, Schieffer RL, Stanton JS, Sebree SK, Verstraeten IM, 2003: Water in Storage and Approaches to Groundwater Management, High Plains Aquifer, 2000. U.S. Geological Survey Circulation 1243

Mesinger, F., and Coauthors, 2006: North American Regional Reanalysis, *Bull. Amer. Meteor. Soc.*, **87**, 343-360.

Miller, J. A., and C. L. Appel, 1997: U.S. Geological Survey, Hydrologic Atlas 730-D. U.S. Geological Survey, Reston, VA, USA.

Moore, N. and S. Rojstaczer, 2002: Irrigation's influence on precipitation: Texas High Plains, U.S.A. *Geophys. Res. Lett.*, **26**, 16, 1755-1758.

Niyogi, D., T. Holt, S. Zhong, P. C. Pyle, and J. Basara, 2006: Urban and land surface effects on the 30 July 2003 mesoscale convective system event observed in the Southern Great Plains. *J. Geophys. Res.*, **111**, D19107.

Paegle, J., K. C. Mo, and J. Nogués-Paegle, 1996: Dependence of simulated precipitation on surface evaporation during the 1993 United States summer floods. *Mon. Wea. Rev.,* **124**, 345-361.

Peel, M. C., B. L. Finlayson, T. A. McMahon, 2007: Updated world map of the Koppen-Geiger climate classification. *Hydrol. Earth Syst. Sci.,* **11**, 1633-1644.

Pielke, R. A., 2005: Land use and climate change. *Science,* **310**, 1625-1626.

Pielke, R. A. and coauthors, 2007: An overview of regional land-use and land-cover impacts on rainfall. *Tellus*, **59B**, 587-601.

Puma, M. J. and B. I. Cook, 2010: Effects of irrigation on global climate during the 20th century. *J. Geophys. Res.*, **115**, D16120.

Sacks, W. J., B. I. Cook, N. Buenning, S. Levis, J. H. Helkowski, 2009: Effects of global irrigation on near-surface climate. Clim. Dyn. **33**, 159-175.

Segal, M., R. Avissar, M. C. McCumber, and R. A. Pielke, 1988: Evaluation of vegetation effects on the generation and modification of mesoscale circulations. *J. Atmos. Sci.*, **45**, 16, 2268-2292.

Segal, M., Z. Pan, R. W. Turner, and E. S. Takle, 1998: On the potential impact of irrigated areas in North America on summer rainfall caused by large-scale systems. *J. Appl. Met.*, **37**, 325-331.

Skamarock, W. C., J. B. Klemp, J. Dudhia, D. O. Gill, D. M. Barker, W. Wang, and J. G.

   Powers, 2005: A Description of the Advanced Research WRF Version 2. NCAR

   technical note, NCAR/TN-468+STR.

Smith, R. B., 1984: A theory of lee cyclogenesis. *J. Atmos. Sci.*, **41**, 1159-1168.

Solomon, S., G. Plattner, R. Knutti, and P. Friedlingstein, 2009: Irreversible climate

   change due to carbon dioxide emissions. *Proc. Natl. Acad. Sci. USA*, **106**, 1704-1709.

Stephens, G. L., 2005: Cloud feedbacks in the climate system: A critical review. *J.

   Climate*, **18**, 237-273.

Suyker, A. E. and S. B. Verma, 2009: Evapotranspiration of irrigated and rainfed maize-

   soybean cropping systems. *Agric. For. Meteorol*, **149**, 443-452.

Trier, S. B., C. A. Davis, D. A. Ahijevych, M. L. Weisman, and G. H. Bryan, 2006:

   Mechanisms supporting long-lived episodes of propagating nocturnal convection

   within a 7-day WRF model simulation. *J. Atmos. Sci.*, **63**, 2437-2461.

Trier, S. B., C. A. Davis, and D. A. Ahijevych, 2010: Environmental controls on the

   simulated diurnal cycle of warm-season precipitation in the continental United States.

   J. Atmos. Sci., **67**, 1066-1090.

Tuttle, J. D., and C. A. Davis, 2006: Corridors of warm season precipitation in the central

   United States. *Mon. Wea. Rev.*, **134**, 2297-2317.

Twine, T. E., C. J. Kucharik, and J. A. Foley, 2004: Effects of land cover change on the

   energy and water balance of the Mississippi River basin. *J. Hydrometeor.*, **5**, 640-655.

Vilsack, T. and C. Z. F. Clark 2009: 2007 Census of Agriculture. United States

Department of Agriculture Report AC-07-A-51. U.S. Department of Commerce,

National Processing Center Jeffersonville, IN.